Title
CHANNEL MODEL OF FLOW THROUGH FRACTURED MEDIA

Authors
Tsang, Y.W.
Tsang, C.F.

Publication Date
1986-04-01

LBL-21310
Preprint

Lawrence Berkeley Laboratory
UNIVERSITY OF CALIFORNIA

EARTH SCIENCES DIVISION

Submitted to Water Resources Research

CHANNEL MODEL OF FLOW THROUGH FRACTURED MEDIA

Y.W. Tsang and C.F. Tsang

April 1986

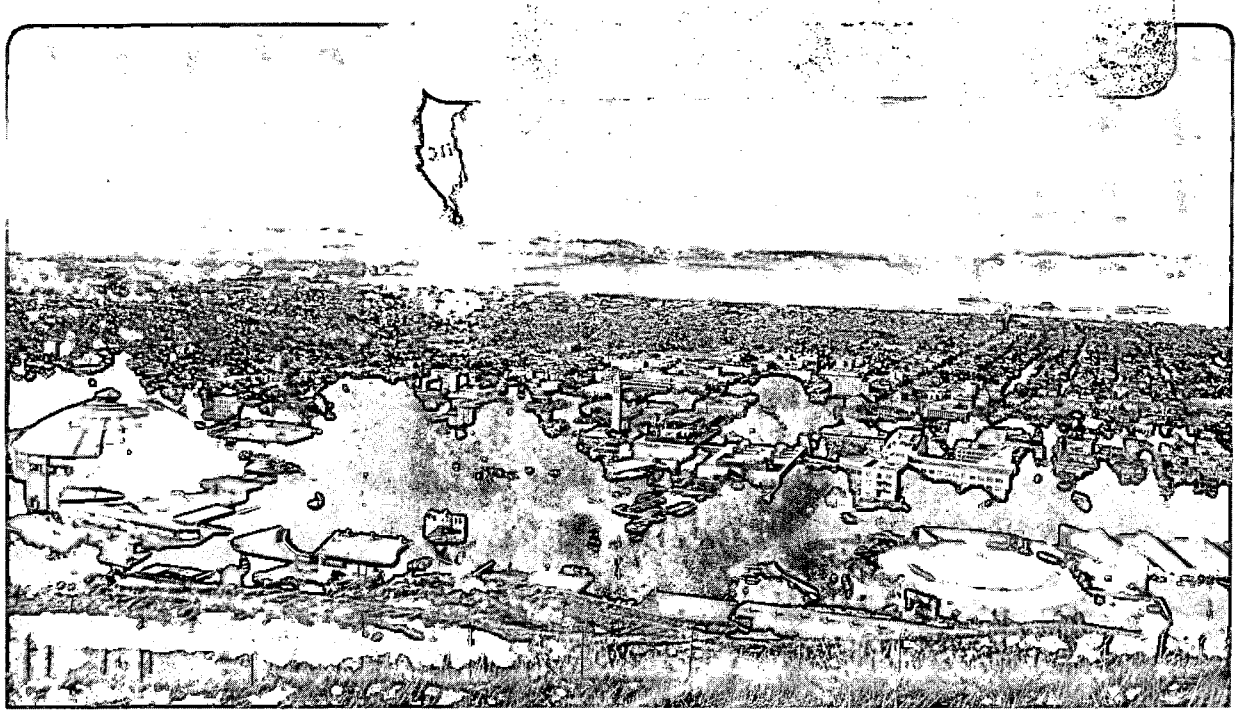

Prepared for the U.S. Department of Energy under Contract DE-AC03-76SF00098

DISCLAIMER

Channel Model of Flow Through Fractured Media

Y. W. Tsang and C. F. Tsang

Lawrence Berkeley Laboratory
Earth Sciences Division
University of California
Berkeley, California 94720

ABSTRACT

Based on a review of recent theoretical and experimental studies of flow through fractured rocks, we have studied the fluid flow and solute transport in a tight fractured medium in terms of flow through channels of variable aperture. The channels are characterized by a aperture density distribution and a spatial correlation parameter. Aperture profiles along the channels are statistically generated and compared to laboratory measurements of fracture surfaces. Calculated tracer transport between two points in the fractured media is by way of a number of such channels. Tracer breakthrough curves display features that correspond well with recent data by Moreno et al., which lends support to the validity to our model. Calculated pressure profiles along the channels suggest possible measurements that may be useful in identifying the geometrical characteristics of the channels. Finally, predictions were made for tracer breakthrough curves in the case of single fracture under various degree of normal stress. These suggested possible laboratory experiments which may be performed to validate this conceptual model.

INTRODUCTION

Recent concerns in the geological isolation of nuclear waste and in deep injection of liquid toxic waste have stimulated much interest in the study of fluid flow and solute transport through tight rocks. Flow through such low permeability rocks predominantly occur in interconnecting fractures. Earlier studies of fracture hydrology (Snow, 1969; Wilson, 1970) have idealized each fracture an a pair of smooth parallel plates separated by a constant aperture, and thus the fluid flowrate varies as the cube of the constant separation. However, a real fracture in rock masses has rough-walled surfaces, and unlike parallel plates, portions of the fracture may be blocked by filling material or closed when subjected to normal stress. Results of laboratory experiments (Engelder and Scholz, 1981; Gale, 1982; Witherspoon et al., 1980) show that the parallel plate approximation for the fracture begins to breakdown at elevated normal stress ($>$10MPa) across the fracture.

The relationship of fracture wall roughness to the fluid flowrate though a single fracture subject to normal stress has been analyzed in a series of theoretical papers (Tsang and Witherspoon, 1981; Tsang and Witherspoon, 1983; Tsang, 1984). Their investigations show that only at low applied stress, when the fracture is essentially open, does the parallel-plate idealization adequately describe fluid flow. As the contact area between the fracture surfaces increases with stress, either applied or in situ, fracture surface roughness ceases to be a mere perturbation on a mean parallel-plate aperture, and the parallel-plate picture is no longer an adequate description of the fracture. Rather, the fracture needs to be mathematically described by the aperture density distribution, n(b), where n(b)db gives the probability of finding apertures with values between b and (b+db). Furthermore, because of the contact areas and constrictions of the fracture subject to stress, flow through a single fracture becomes a two-dimensional flow through a few channels which are tortuous, have variable aperture along their length, and which

may or may not intersect each other (Tsang, 1984). The field experiment of Abelin et al. (1983) on a single fracture showed that the equivalent fracture aperture derived from the constant head permeability measurements was a few orders of magnitude smaller than that derived from the tracer migration experiments. The equivalent apertures derived from these two different measurements should be identical if the parallel-plate description of the fracture were valid. However, if in fact fracture roughness and constrictions limit the flow only to a few tortuous channels, then the permeability measurements would be controlled by the small apertures and constrictions, and therefore by tortuosity. On the other hand, the tracer breakthrough time samples the total volume of the channel. The net consequence would be a significant discrepancy between the two "equivalent parallel-plate aperture" as reported by Abelin et al. (1983), if the data were analyzed in terms of the parallel-plate model. More recently, Pyrak et al., (1985) performed experiments in which they injected molten wood's metal into single fractures, and obtained direct evidence for the formation of tortuous channels in single fractures as different levels of normal stress were applied. Observations of tracer transport in single fractures in the Stripa mines (Neretnieks, 1985) showed that the time and amount of tracer returns at two near-by sampling points were very different, and this lends support to the channel nature of fluid flow through fractured media.

THE CHANNEL MODEL

On the basis of theoretical and experimental observations referred to above, we study here the fluid flow and solute transport in a tight fractured medium in terms of flow through channels of variable apertures. The channel flow model is conceptually different from the current approaches to the problem of flow through a fractured medium, which can be broadly classified into two categories. One approach is to treat the fractured medium as an equivalent porous medium. This is appropriate when the fractured medium contains many inter-connecting fractures. The second approach treats the flow through a number of discrete fractures. In the porous medium approximation, the key parameters are the equivalent permeability tensor for fluid flow (Hsieh et al., 1985; Neuman et al., 1985), and the dispersivity for solute transport. The dispersivity is traditionally considered to be a spatial invariant in a porous medium (Bear, 1972). In fact, there is much field evidence that the dispersivity is not a constant due to medium heterogeneities, but depends on the travel distance and/or scale of the system. Several workers have taken different approaches to incorporate the scale dependent dispersion in modeling studies (e.g., Sauty et al.,1979; Gelhar et al.,1979; Pickens and Grisak, 1981).

For cases where the medium is tight and fracture intersections are few, a discrete representation of the fractures has been used in the problem of flow and transport (for example, Long and Witherspoon, 1985; Long, et al., 1982; Robinson, 1983; Schwartz, et al., 1981; Smith and Schwartz, 1980). Though these authors treat the problem in different ways they all start with the common assumptions that the single fracture is the basic unit for the fractured medium, and that each fracture is represented by a pair of parallel plates with a constant aperture. On the basis of distributions of fracture aperture, fracture length, fracture spacing, and fracture orientation they generate a statistical model for the fracture network. Since the physical laws governing the flow and transport through a pair of smooth parallel plates are known, transport and flow through the

fracture network can be computed. The interesting question of the connectivity of the fracture networks with regard to flow has been raised by these studies. For fractured porous medium where the effect of the rock matrix cannot be ignored, numerical models such as the double porosity method (Warren and Root, 1963; Duguid and Lee, 1977) and the multiple interacting continua (MINC) method (Pruess and Narasimhan, 1982) have been proposed, but these methods also adopt the parallel-plate description of each single fracture. However, based on the studies on single fracture as discussed earlier, the parallel-plate representation of the single fracture is not realistic. If one were to include the effect of roughness, one would also need to include distributions for aperture and the degree of contact between the fracture surfaces. Then it becomes impractical to use the single fracture as the basic unit in modeling a fractured medium. We therefore propose in this paper to abandon the single fracture as the starting point to model a fractured medium.

Instead we will represent the fluid flow and solute transport through a tight rock medium by means of a limited number of tortuous and intersecting channels. These channels have variable apertures along their lengths. The parameters that characterize the channels are (1) the aperture density distribution, which gives the relative probability of the occurrence of a given aperture value, (2) the effective channel length and (3) the aperture spatial correlation length, which gives the spatial range within which the aperture values are correlated. In the channel representation there is no physical basis to distinguish flow through a single fracture from flow through the connected fractures in a multiple-fracture network. Based on these considerations, we start with an aperture distribution and a spatial correlation parameter. From these, systems of channels can be generated using geostatistical methods. Based on the flow through these channels, predictions of (1) the expected steady-state pressure variation in the fractured medium under constant pressure boundary conditions, and (2) the tracer concentration as a function of time in tracer transport measurements may be calculated. Comparisons of these

theoretical predictions existing experimental data in the literature were made. The results led us to believe that this new approach of representing fluid flow through a fractured medium by channel flow is promising. The calculations we present in this paper will be the first in a series based on this channel flow model. Results presented are from the forward calculation; namely, predictions on pressure and transport based on a given set of aperture density distribution and spatial correlation parameter. A thorough understanding of the forward problem is needed in order to proceed to the solution of the inverse problem, in which values of these parameters are deduced based on pressure and tracer transport data.

CHANNEL APERTURE PROFILES

Implicit in the channel model of fluid flow is that the fluid avoids the constrictions and filled areas of the fracture, so the flow paths are comprised of only the "open" (non-zero apertures) part of the fracture. Figure 1 shows schematically the channeling effect in a single fracture. Figure 2 shows schematically the channeling effect in a number of three-dimensional intersecting fractures. Note that the channels in Figure 1 or Figure 2 may flow independently of or cross each other. Each channel in Figure 1 or 2 is represented schematically in Figure 3. It is defined by the aperture density distribution n(b) along its length. The channel width is assumed to be a constant of the same order as the correlation length, λ, since, by definition, the correlation length is the spatial range within which the apertures have similar values. The channel length does not equal the linear length between two points, but it is not expected to vary more than a factor of two to three from the actual linear length.

We now describe the procedure to generate channels that are consistent with a given aperture distribution and a specified correlation length. If the aperture density distribution were uniform, there exists a standard prescription in geostatistical methods (for example, Journel and Huijbregts, 1978) to generate one-dimensional channels with

variable apertures and a spatial correlation length, λ. The procedure is described briefly as follows. One starts with a set of numbers $T(x_i)$ drawn randomly from the uniform distribution U [-0.5,0.5] and placed on equidistant points, x_i, on a line. The equidistant spacing is $\Delta x = \lambda/n$ where λ is the range of correlation and n an integer. Journel and Huijbregts (1978) suggest that n should be at least 20. The distribution $T(x_i)$ thus generated is of course spatially uncorrelated. If a moving and weighted average is performed over the correlation range, λ , on $T(x_i)$, a uniform distribution with correlation, $Y(x_i)$, will be derived. The form of the weighted function used in the averaging procedure depends on the variogram of the aperture variation. In this paper, we assume an weighted function consistent with a spherical variogram. The distribution $Y(x_i)$ has a mean value 0 and variance $n(n+1)(2n+1)/36$. One can derive from $Y(x_i)$ a normal distribution with the same correlation range, λ, but with mean μ and variance σ^2, The normal distribution, $Z(x_i)$, is,

$$Z(x_i) = Y(x_i)\frac{\sigma}{\sqrt{n(n+1)(2n+1)/36}} + \mu. \qquad (1)$$

The above standard procedure is applicable therefore to distributions that are uniform, normal or log normal. Since field measurements of apertures may not always fall into one of the above distributions, we introduce the following transformation so that we may statistically generate a channel of correlated apertures, given any aperture distribution. The transformation consists of the following. The cumulative frequency of a normal density distribution of mean 0 and variance 1 is computed. The cumulative frequency distribution of any given aperture density distribution is also computed, either analytically if the density distribution is analytic, or numerically if the density is from measurements. A graphic transformation from the aperture values determined by the normal distribution to the apertures values determined by the actual aperture distribution is then performed by equating the values of the cumulative frequency. A computer subroutine was written to numerically perform the graphic transformation.

We now turn our attention to the question of how one arrives at the aperture distribution and the correlation parameter which characterize the channels. For channels in a single fracture, it seems conceptually reasonable that the aperture distribution and correlation range of the single fracture also describe that of the channels. One possible modification is that since the channel representation of the single fracture has already filtered out the zero and small apertures, an aperture density distribution derived from single fracture data but truncated (on the small aperture end) may be a more appropriate one for the channels. To test the validity of the above hypothesis we carried out geostatistical simulations in two dimensions with a specified aperture distribution and spatial correlation. From the simulated apertures for two-dimensional fractures, channels that avoid zero or small apertures were identified, and their aperture values confirm the above hypothesis that a density distribution for fracture is applicable to channel. For channels spanning intersecting fractures as shown schematically in Figure 2, it is conceivable that the values of the channel parameters vary from fracture to fracture, that is, there exists a spatial drift for both the aperture density distribution and correlation length. Mathematically, there is no intrinsic difficulty in generating channels consistent with the variable aperture density and variable correlation range. The difficulty is in the interpretation and reduction of fracture geometry data such as fracture spacing, fracture length, fracture orientation, and fracture aperture to the few parameters that characterize the equivalent flow channels. On the other hand, it is also conceivable, by the very nature of the channel model which picks out the least resistive flow paths, that there is a "homogeneity" to the properties of the channel so that representative aperture density and correlation length may be determined to characterize the entire region of interest in the field. For the purpose of this paper, where the emphasis is on the theoretical predictions of pressure and concentration measurements based on the channel description of fracture flow, and where the predictions will be qualitatively compared with the experimental data through a single fracture, we will assume that the same

aperture density and correlation is valid over the region of interest.

S. Gentier (personal communication, 1983) measured the fracture roughness profiles of the surfaces of a natural granite fracture 12 cm in diameter. The measurements were taken from both the top and bottom surfaces of the fracture along ten traces, of which five were in one direction, and five in the orthogonal direction. The two fracture surfaces are matched, so the difference of the measurements for the top and bottom surfaces gives the apertures. When all the apertures measurements over the fracture were pooled together, it was found (Tsang, 1984) that the aperture density distribution (Fig. 4b) can be approximated by a Gamma function (Fig. 4a):

$$n(b) = \frac{1}{b_o^2}\, b\, e^{\frac{-b}{b_o}} \tag{2}$$

The distribution peaks at b_o, the only parameter in the Gamma function; the mean aperture is 2 b_o. We have computed variograms for the measured apertures along each trace, and have estimated the range in the variograms to be between 0.1 and 0.2 of the trace length. Since our prescription to generate statistically equivalent realizations of channels of variable aperture holds for any aperture distribution and correlation parameter, we choose for our calculations the density distribution to be the Gamma function with $b_o = 40\ \mu m$, and the correlation length, λ , to be 0.2 times the channel length.

Applying the prescription as we have outlined earlier, different realizations of the channels with the chosen aperture density distribution and correlation length may be generated. Three of these generated realizations are shown in Figure 5. For comparison, Figure 6 shows some aperture profiles derived from the data of Gentier as discussed earlier. The qualitative similarity between the statistically generated channel and the measurements is remarkable. The absolute values of the apertures differ in Figures 5 and 6 because the b_o is chosen to be 40 μm for our calculations here, but is of the order of 100 μm in the experimental data in Figure 6. In Figure 7, we show a few statistically generated channels with identical aperture density distribution but with correlation

parameters of $\lambda/L = 0.2$, 0.1 and 0.05. The contrast between the three different profiles in Figure 7 brings out the significance of the spatial correlation.

When a pressure head difference is applied between two points, the flow paths between these two points may be represented by a number of channels, which may intersect each other at various points (Fig. 8a). Figure 8b shows two channels with one crossover. Under steady state flow conditions, the flow through the two intersecting channels may be approximated by the flow through three independent, non-intersecting channels. The flow through each of these three channels is regulated by the same aperture distribution and correlation length along the channels. Their widths, on the other hand, are defined such that the flow rate q is conserved. With every crossover, there is the added possibility of a different flow path. Recall that the channels are statistically generated to be consistent with an aperture density and a correlation length which supposedly characterize the flow paths in the fractured medium. It is therefore conceptually acceptable to represent statistically a system of m intersecting channels by a set of $M>m$ independent channels that do not cross each other; since by definition all the channels are statistically equivalent. The more crossover there are in the system of intersecting channels, the larger will M be as compared to m. In the above, we have assumed that all the channels that originate from 1 converge to 2. This need not be the case. Consider the situation shown in Figure 8c: one of the channels that originate from the higher pressure point 1 was "lost" on the way to the lower pressure point 2. Then instead of sampling two possible flow paths between 1 and 2, tracer transport measurements "see" effectively only one flow channel. The fact that all the flow channels are statistically equivalent again comes in handy, so that we may represent the physical situation in Figure 8c by one independent channel. In summary, the system of M independent flow channels such as schematically shown in Figure 8d encompasses all the physical channel configurations of Figures 8a-8c as far as the statistical predictions of pressure and tracer transport measurements are concerned. The formulas for tracer concentration and pressure given below

will be based on the system of M independent channels as shown in Figure 8d.

TRACER CONCENTRATION BREAKTHROUGH CURVES

Suppose tracer of concentration C_o is injected at the high pressure end, the breakthrough tracer may be measured at the low pressure exit in the form of $C(t)/C_o$. For one given channel i, $C_i(t)/C_o$ is to a good approximation given by a step function $H(t-t_i)$ where $H(x)=0$ for $x<0$ and $H(x)=1$ for $x\geq 0$, and where t_i is the breakthrough time for channel i. The Taylor's dispersion will smear out the sharp edge of the step-function. The flow velocity in each channel is controlled mainly by the small apertures along the channel. The breakthrough time depends on integrated volume of the channel divided by the flow velocity. It is straightforward to show that

$$q_i = \frac{1}{\mu}\left(\sum_j \frac{12\Delta x}{b_{i,j}^3}\right)^{-1} \lambda(P_1 - P_2) \tag{3}$$

$$t_i = \frac{\mu}{(P_1 - P_2)}\left(\sum_j b_{i,j}\,\Delta x\right)\left(\sum_j \frac{12\Delta x}{b_{i,j}^3}\right) \tag{4}$$

where $b_{i,j}$ is the j-th aperture value in the discretized interval Δx along the channel i, and where q_i is the steady state mass flow of the channel i. For a system of M independent channels, as shown in Figure 8d, the tracer concentration as a function of time is given by:

$$\frac{C(t)}{C_o} = \frac{\sum_{i=1}^{M} q_i\, H(t-t_i)}{\sum_{i=1}^{M} q_i}. \tag{5}$$

Note that in the above discussion, we have not accounted for the presence of rock matrix in which the fractures are embedded. Matrix effects should not be neglected in problems of solute transport because of the possibility of matrix diffusion, a particularly important effect when the travel distance is large. Matrix diffusion can be incorporated

into our present model with very little added effort. Its effect is to retard the solute arrival time from each channel by different amounts depending on the velocities in each channel, and to 'smear out' the breakthrough front. Since we will present in this paper the first set of calculations employing the channel model, and since we will compare our calculations to data from laboratory studies only, the effect of matrix diffusion will not be included.

Equations (3) through (5) are evaluated for a number of arbitrarily chosen values of M, the total number of channels. Each channel obeys the same aperture distribution (Fig. 4b) with $b_o = 40\mu m$, and has the same correlation length of 0.2 L. Figures (9a) through (9e) show the concentration as a function of time for M = 33, 32, 16, 11 and 8, respectively. The values shown on the x axis should be multiplied by $12L^2\mu \cdot 10^{12}/(P_1-P_2)$ (in SI units) in order to get the proper time units in seconds. We note a rather steep rise in the concentration curves in the early times, then some "stair-step" structure, due to the finite delay for the solute carried in the next channel to breakthrough. The early arrivals correspond to flow in fast channels, those with large apertures. The steep rise therefore indicates that a large proportion of the statistically generated channels have large apertures. In Figures (10a) through (10d) we reproduce the breakthrough curves from laboratory experiments (Moreno et al, 1985) performed on a single fracture in a 19.5 cm core. Breakthrough curves are usually analyzed in the context of solutions to advection-dispersion equations, and parameters are adjusted to fit a smooth dispersion-advection curve through the data. In Figure 10 we have copied only the data points. On careful examination of Figures 9 and 10, it appears that the prominent features in the theoretical curves based on the channel model (Fig. 9) are also evident in Figure 10. These features (such as the steep rise in tracer returns and the stair-step structures) are not found in the conventional advection-dispersion curves. This observation lends support to the channel representation of the fluid flow in fractures. An interesting case for comparison is the tracer concentration breakthrough curves when each of the

independent channels has a constant aperture, and the apertures of the channels sample the aperture distributions function down to a truncation value of b_{min} (i.e., the apertures sampled are $b > b_{min}$). Figure 11 shows the results for $b_{min} = 0.1b_o$, $2b_o$ and $3b_o$. The curves are found to be smooth, their slopes and times for $C(t)/Co=1$ are strongly dependent on b_{min}. Note also that the initial breakthrough times are several order smaller than in the case where each channel has variable aperture. The variation of apertures along each channel brings in the effect of constriction which slows down the breakthrough. It is therefore important to take into account the variation of aperture values along the length of each channel when describing fluid flow in fractures in terms of channeling.

On the basis of the channel model, parameters for channel flow may be back-calculated from the breakthrough data. Let us assume that the experimental breakthrough data (Moreno et al, 1985) in Figure 12a may be analyzed in terms of breakthrough from a set of independent channels. We took the differences between consecutive data points (assuming that the first non-zero data point at $t \approx 2$ minutes to be within error bar of zero value). These differences are a measure of the flow, q_i, carried in one channel or a group of channels that are bunched in the arrival time. The flow q_i as a function of travel time is plotted in Figure 12b. The product of q_i and travel time gives the volume, v_i, of each channel and v_i is plotted in Figure (12c). The back-calculated values are only integrated properties of the entire channel, yet these quantities can be quite useful. They will be used in a later section of the paper to predict the behavior of tracer breakthrough when the fracture is subject to different levels of normal stress. For comparison, we include in Figure 13 the volume, of each channel versus arrival time for 33 statistically generated channels. We note that these statistically equivalent channels have very similar volumes. If we assume in Figure 12c that the volume unit corresponds to the smallest column (at $t \approx 4$ min); and that higher columns represent a bunching together of several channels, each with the same volume unit, then there are a large number of channels at early times. Between the first arrival of tracer

concentration at t≈3 mins and t≈6 mins, there are probably 16 channels. Then 3 channels occur at t≈7.7 min and 2 channels at t≈8.7 min. Such bunching of channels is evident in the theoretical results in Figure 14, though direct comparison cannot be done, since we do not have the aperture distribution of the laboratory sample.

PRESSURE MEASUREMENTS IN FRACTURED MEDIUM

The pressure distribution along each channel is given by:

$$P(x) = (P_1 - P_2) \frac{\int_0^x \frac{dx}{b^3(x)}}{\int_0^L \frac{dx}{b^3(x)}}, \qquad (6)$$

where L is the total channel length and x equals 0 at P_1 and x equals L at P_2. In Figure 14 we show the normalized pressure profiles along the four different channels labeled (a) through (d), one of which ((a)) has the aperture variation along the channel corresponds to the one shown in Figures 7a. The sharp drops in the pressure profiles correspond to locations of aperture constrictions. If the fluid flow between P_1 and P_2 is through a constant aperture single fracture, or through a network of dense fractures that can be approximated by a porous medium, then the steady state pressure measurements should follow a straight line from P_1 to P_2. On the other hand, if the flow between P_1 and P_2 is in fact through a set of intersecting, tortuous channels of variable apertures, then pressure measurements carried out in a observation borehole at a particular intermediate point, x, between P_1 and P_2 can give very different values at different packed intervals, and each value can also deviate very much from that predicted by the linear drop from P_1 to P_2. This is clearly indicated by the possible pressure profiles shown in Figure 14. How the measured values differ from a straight line depends on the ratio of the integrated effects of aperture constrictions along the particular channel on the two sides of the observation well that intercepts it. If the measured value is above that

predicted by the straight line, then the amount of aperture constrictions from P_1 to x is smaller than that from x to P_2. On the other hand, if the measured value is well below that predicted by the straight line, then small apertures tend to bunch in the part of channel between P_1 and x. This implies that if a pressure packer test is performed in an observation borehole that intercepts a number of channels, these channels may display different pressure heads, even though they are connected. Referring to Figure 14, where, if the observation borehole is located half way between P_1 and P_2 (0.5 on the x axis), packered pressure measurements on the four channels a, b, c, and d will give pressure head values of 0.3, 0.8, 0.02 and 0.7 (P_1–P_2) respectively.

Recall in the discussion of our approach to the channel flow model for a set of intersecting fractures, the question of whether there is a spatial drift to the aperture density and correlation parameter was raised. It seems that pressure packer test performed at distances both larger and smaller than a typical fracture size in the medium may shed some light on this question. The presence of a spatial drift in the aperture density will be indicated by packer measurements consistently higher or lower than that predicted by linear interpolation between P_1 and P_2.

In both the breakthrough times and the pressure profiles, we have presented results calculated from a particular choice of aperture density distribution and correlation parameter. A different correlation parameter will give very different spatial variation of the apertures of each channel as shown in Figures 5 and 7. However, the resultant breakthrough tracer curves all have the same common characteristic and it is not possible to differentiate the results even if the correlation parameter is reduced to 0.05. That the tracer breakthrough should be insensitive to the value of the spatial correlation is not surprising since both the flow and breakthrough times are dependent on the integrated values of some functions of the apertures over the entire channel. The question of how the form of aperture density distribution will affect the shapes and characteristics of the breakthrough curves within the framework of this channel representation of fluid flow

remains to be studied. Similarly, different values of correlation parameter have little effect on the pressure profiles. Profiles very similar to those shown in Figure 14 were obtain for channels with aperture spatial correlation equals to 0.05 of the channel length. We attribute the insensitivity of pressure measurement to the spatial correlation again to the integrated nature of the mathematical formula for the pressure.

TRACER BREAKTHROUGH CURVES AS A FUNCTION OF NORMAL STRESS

When normal stress across a fracture is increased, the reduction in channel apertures affects the tracer breakthrough curves. Consider tracer transport through 33 channels whose apertures are reduced by 0, 2, 4 and 6 μm respectively (Fig. 15). Calculations are straightforward and results are presented in Figure 16a-c. Figure 15a is identical to Figure 9a. As apertures are reduced, tracer breakthrough times of the channels increase acccording to equation (4). In all the cases calculated (Fig. 15a-d), the same number of channels are assumed, but the breakthrough times of the slower channels are too long to be shown in the figures on the large aperture-reduction cases. The step features persist and actually become more significant at values of higher stress. This kind of correlation of breakthrough curves with changes in normal stress may be a good test of the validity of the channel model. In such a test, one may start with the experimental breakthrough data (Fig. 12) and back-calculate the integrated parameters q_i and v_i as discussed earlier. Then the linear closure, δ , of the fracture as a result of applied stress may be measured. If the volume of each channel, v_i, is assumed to become $(v_i - \delta\lambda L)$, where λ is the correlation length and L is the effective length of the channel; and if the flowrate through the channel is assumed to be controlled by the smallest channel constriction, it can be shown that q_i becomes approximately $[(q_i/\alpha)^{1/3} - \delta]^3$, where α is a constant given by $\rho g/12\mu\,(P_1 - P_2)$. For the case where the closure reduces the mean aperture value by 6%, a new predicted tracer breakthrough curve can be calculated from the initial data from

Figure 12. The prediction is shown in Figure 16. If we compare this figure with Figure 12, it is apparent that because of the smaller flow rates, the tracer concentration curve shifts to larger times, with the breakthrough time of the slowest channel shifted off scale in Figure 16c. Note than even with such a small change in the mean fracture aperture, a large change in the breakthrough curve is expected. The reason is that the small change affects significantly the constricted part of the channels, which controls the flow rates. The prediction of these large changes in breakthrough curves can be tested against actual measurements of the breakthrough curves for different level of normal stress. We believe that this is a feasible experiment, and a crucial one if one were to gain confidence in this entirely new approach of studying flow through fractures in terms of channels.

CONCLUSION

We have attempted to understand and calculate transport through fractured media in terms of flow through interconnected channels. Th^ channels can be characterized by an aperture density distribution function and a spatial correlation parameter. In this initial study, the aperture density distribution function is represented by a Gamma function consisting of one parameter. Thus with two parameters the channels are defined with statistically generated aperture profiles. Tracer transport between two points in the fractured media is by way of a number of such channels. Calculated tracer breakthrough curves have features that correspond well to those in recent data by Moreno et al., which lends support to the validity to our model. Calculated pressure profiles along the channels suggest possible measurements that may be useful in identifying the geometrical characteristics of the channels. Both the tracer breakthrough and pressure profile seem to be not sensitive to the value of spatial correlation chosen. Their dependence on the form of aperture distribution remains to be studied. Finally, predictions were made for tracer breakthrough curves in the case of single fracture under various degree of normal stress. These suggested possible laboratory experiments which may be

performed in order to validate this conceptual model.

Validation of this conceptual model by experiments is crucial, since we have made a number of simplifying assumptions in our approach, in order to side-step the issues of the very complicated geometry involved in the flow through a three-dimensional multi-fracture system. The appeal of this approach lies in its simplicity. The flow through a multi-fractured medium is described only in terms of apertures and their spatial correlation. Since the spatial correlation parameter corresponds to that of the variation of apertures in the rough-walled fracture, it is small compared to the fracture geometry parameters such as fracture spacing and fracture size. This small correlation length is the reason why the statistical approach is valid. Thus, it is possible to sample the apertures at different locations over the region of interest in order to yield statistically meaningful parameters for the channel model. The channel length, on the other hand, does depend on the fracture network parameters. For tight systems where fracture spacings and sizes are comparable to the characteristic distances of measurements, statistical approach is not valid, and the channel length needs to be treated as a deterministic quantity to be deduced from pressure and tracer test through the solution of an inverse problem.

ACKNOWLEDGMENTS

Assistance from Frank V. Hale III in computation and graphics is gratefully acknowledged. The careful review and comments by Drs. J. S. Y. Wang and N. E. Goldstein are much appreciated. This work was supported through U.S. Department of Energy Contract No. DE-AC03-76SF00098 by the Assistant Secretary for Energy Research, Office of Basic Energy Sciences, Division of Engineering and Geosciences.

REFERENCES

Abelin, H., J. Gridlund and I. Neretnieks, Migration experiments in a single fracture in the Stripa granite: Preliminary results, in Proceedings of the Workshop on geological Disposal of Radioactive Waste in Situ Experiments in Granite, Stockholm, Sweden, pp. 154-163, Organization for Economic Cooperation and Development, Paris, 1983.

Bear, J., Dynamics of fluids in porous media, 764 pp., Elsevier, New York, 1972.

Billaux, D., B. Feuga and S. Gentier, Etude theorique et en laboratoire du comportment d' une fracture rocheuse sous contrainte normale, Rev. Fr. Gestech. n. 26, first quarter, 1984.

Duguid, J. O. and P. C. Y. Lee, Flow in fractured porous media, *Water Resour. Res.*, 13(3), 758-566, 1977.

Engelder, T. and C. H. Scholz, Fluid flow along very smooth joints at effective pressure up to 200 megapascals, in Mechanical Behavior of Crustal Rocks, Geophys. Monogr., Vol. 24, edited by N. L. Carter, et al., pp. 147-152, AGU, Washington, D. C., 1981.

Gale, J. E., The effects of fracture type (induced versus natural) on the stress-fracture closure-fracture permeability relationships, Proceedings at 23rd Symposium on Rock Mechanics, The University of California, Berkeley, California, 290-298, 1982.

Gelhar, L. W., A. L. Gutjahr, and R. L. Naff, Stochastic analysis of macro dispersion in a stratified aquifer, *Water Resour. Res.*, 15(6), 1387-1397, 1979.

Gentier, S., private communication, 1983.

Hsieh, P. A., S. P., Neuman, G. K. Stiles and E. S. Simpson, Field determination of the three-dimensional hydraulic conductivity tensor of anisotropic media, 2, Methodology and Application, Methodology and Application to Fractured Rock, *Water Resour. Res.*, 21(11), 1667-1676, 1985.

Journel, A. G. and C. T. Huijbregts, Mining geostatistics, 600 pp. Academic Press, New York, 1978.

Long, J. C. S., Investigation of equivalent porous medium permeability in networks of discontinuous fractures, Ph.D. Thesis, University of California, Berkeley, CA, 1983.

Long, J. C. S., J. S. Remer, C. R. Wilson, and P. A. Witherspoon, Porous media equivalent for networks of discontinuous fractures, *Water Resour. Res.*, 18(3), 645-658, 1982.

Long, J. C. S. and P. A. Witherspoon, The relationship of the degree of interconnection

to permeability of fracture networks, *J. Geophys. Res.,* 90(B4), 3087-3098, 1985.

Moreno, L., I. Neretnieks and T. Eriksen, Analysis of some laboratory tracer runs in natural fissures, *Water Resour. Res.,* 21(7), 951-958, 1985.

Neretnieks, I., Transport in fractured rocks, Proceedings, Memoires of the 17th International Congress of IAH, Tuscon, AZ, Vol. XVII, 301-318, 1985.

Neuman, S. P., E. S. Simpson, P. A. Hsieh, J. W. Jones and C. L. Winter, Statistical analysis of hydraulic test data from fractured crystalline rock near oracle, Arizona, Proceedings, Memoires of the 17th International Congress of IAH, Tuscon, AZ, 289-301, 1985.

Pickens, J. F., and G. E. Grisak, Modeling of scale-dependent dispersion in hydrogeologic systems, *Water Resour. Res.,* 17(6), 1701-1711, 1981.

Pruess, K. and T. N. Narasimhan, On fluid reserves and the production of superheated steam from fractured vapor-dominated geothermal reservoirs, *J. of Geophy. Res.,* 87(B11), 9329-2339, 1982

Pyrak, L. R., L. R. Myer and N. G. W. Cooke, Determination of fracture void geometry and contact area at different effective stress, Transactions, American Geophysical Union, 66(903), 1985.

Robinson, P. C., Connectivity of fracture systems--a percolation theory approach, *J. Phys. A:* Math. Gen., 16, 605-614, 1983.

Sauty, J. P., A. C. Gringarten and P. A. Landel, The effect of thermal dispersion on injection of hot water in aquifers, paper presented at the second invitational Well Testing Symposium, U.S. Dept. of Energy, Lawrence Berkeley Laboratory, Berkeley, CA, 1979.

Schwartz, F. W., L. Smith, and A. S. Crowe, Stochastic analysis of groundwater flow and contaminant transport in a fractured rock system, Proceedings Material Research Society, Symposium on the Scientific Basis of Nuclear Waste Management, Boston, 1981.

Smith, L. and F. W. Schwartz, Mass transport, 1, a stochastic analysis of macroscopic dispersion, *Water Resour. Res.,* 16(2), 303-313, 1980.

Snow, D. T., Anisotropic permeability of fractured media, *Water Resour. Res.,* 5(6), 1273-1289, 1969.

Tsang, Y. W. and P. A. Witherspoon, Hydromechanical behavior of a deformable rock fracture subject to normal stress, *J. Geophys. Res.,* 86(B10), 9287-9298, 1981.

Tsang, Y. W., The effect of tortuosity on fluid flow through a single fracture, *Water Resour. Res.,* 20(9), 1209-1215, 1984.

Tsang, Y. W. and P. A. Witherspoon, The dependence of fracture mechanical and fluid

properties on fracture roughness and sample size, *J. Geophys. Res.*, 88(B3), 2359-2366, 1983.

Wilson, C. R., An investigation of laminar flow in fractured porous rocks, Ph.D. Thesis, University of California, Berkeley, CA, 1970.

Witherspoon, P. A., J. S. Y. Wang, K. Iwai and J. E. Gale, Validity of cubic law for fluid flow in a deformable rock fracture, *Water Resour. Res., 16(6), 1016-1024.*

Warren, J. E. and P. J. Root, The behavior of naturally fractured reservoir, *Soc. of Pet. Eng, J.*, 245-255, 1963.

FIGURES

Figure 1. Schematic diagram of the channel representation of fluid flow in a single fracture.

Figure 2. Schematic diagram of the channel representation of fluid flow in a multiple fractured medium.

Figure 3. Schematic sketch for one channel.

Figure 4. (a) Gamma function as the theoretical aperture density distribution.

(b) Experimental aperture density distribution derived from Gentier (personal communication, 1983), and Billaux et al. (1985).

Figure 5. (a)-(c) Statistically generated realizations of the spatial variation of apertures with spatial correlation of 0.15 of channel length.

Figure 6. Aperture variation along three traces in a single fracture derived from the profile measurements for a single granite fracture (Gentier, personal communication, 1983).

Figure 7. (a)-(c) Statistically generated realizations of the spatial variation of apertures with spatial correlation of 0.2, 0.1 and 0.05 of channel length, respectively.

Figure 8. (a) A schematic diagram of fluid flow paths between two points maintained at pressures P_1 and P_2.

(b) A diagram of two intersecting channels.
(c) A diagram of a 'lost' channel between P_1 and P_2.

(d) A set of independent channels, a conceptually equivalent representation to the flow paths shown in 8(a).

Figure 9. (a)-(e) Theoretical tracer concentration breakthrough curves for a set of M channels with common end point pressures P_1 and P_2.

Figure 10. (a)-(d) Tracer concentration breakthrough data from Laboratory measurements on a single fracture in a granitic core 18.5 cm in height and 10 cm in diameter (Moreno et al, 1985). The four curves correspond to different runs involving different injection flow rates and different tracers (NaLS or I).

Figure 11. Tracer concentration breakthrough time for 100 constant-aperture channels when the channel apertures sample the aperture density distribution of Figure 4(a) truncated at $b_{min} = 0.1\ b_o$, $2.0\ b_o$ and $3.0\ b_o$.

Figure 12. (a) An experimental tracer concentration breakthrough curve (from Moreno, et al., 1985).

(b) Derived flowrates in each channel versus breakthrough time.
(c) Derived volume of each channel versus breakthrough time.

Figure 13. Channel volume versus breakthrough time for the 33 statistically generated channels.

Figure 14. Pressure profile along four channels; one of which (labeled (a)) corresponds to the aperture variation shown in Figure 7a.

Figure 15. (a)-(d) Calculated tracer concentration breakthrough curves for the cases where the apertures are reduced by 0, 2, 4 and 6, as a result of applied stress.

Figure 16. Predicted tracer concentration breakthrough curves for flow through a single fracture subject to normal stress, based on the laboratory data shown in Figure 13.

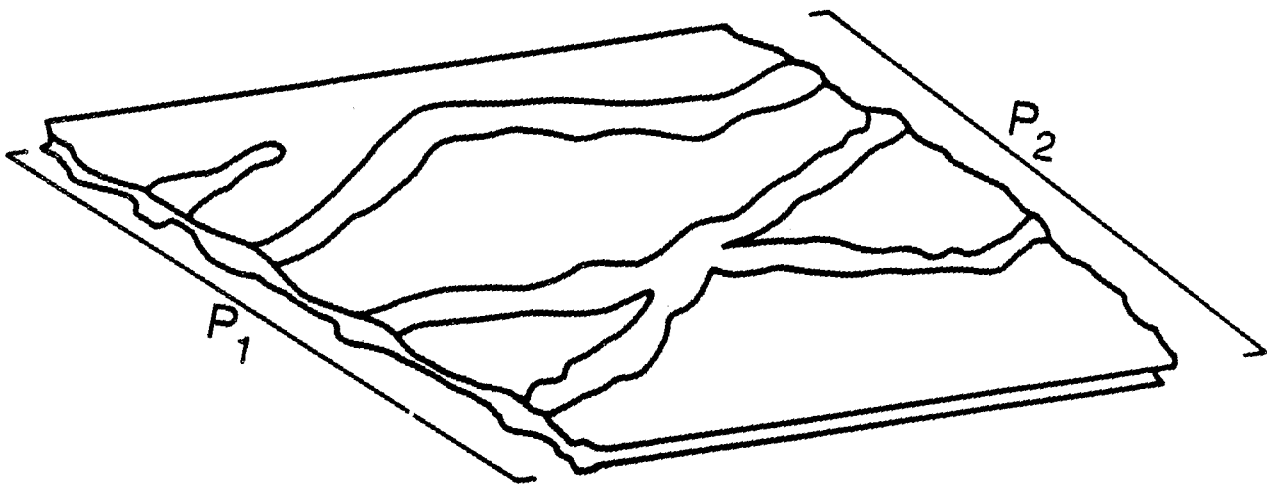

XBL 863-10724

Figure 1.

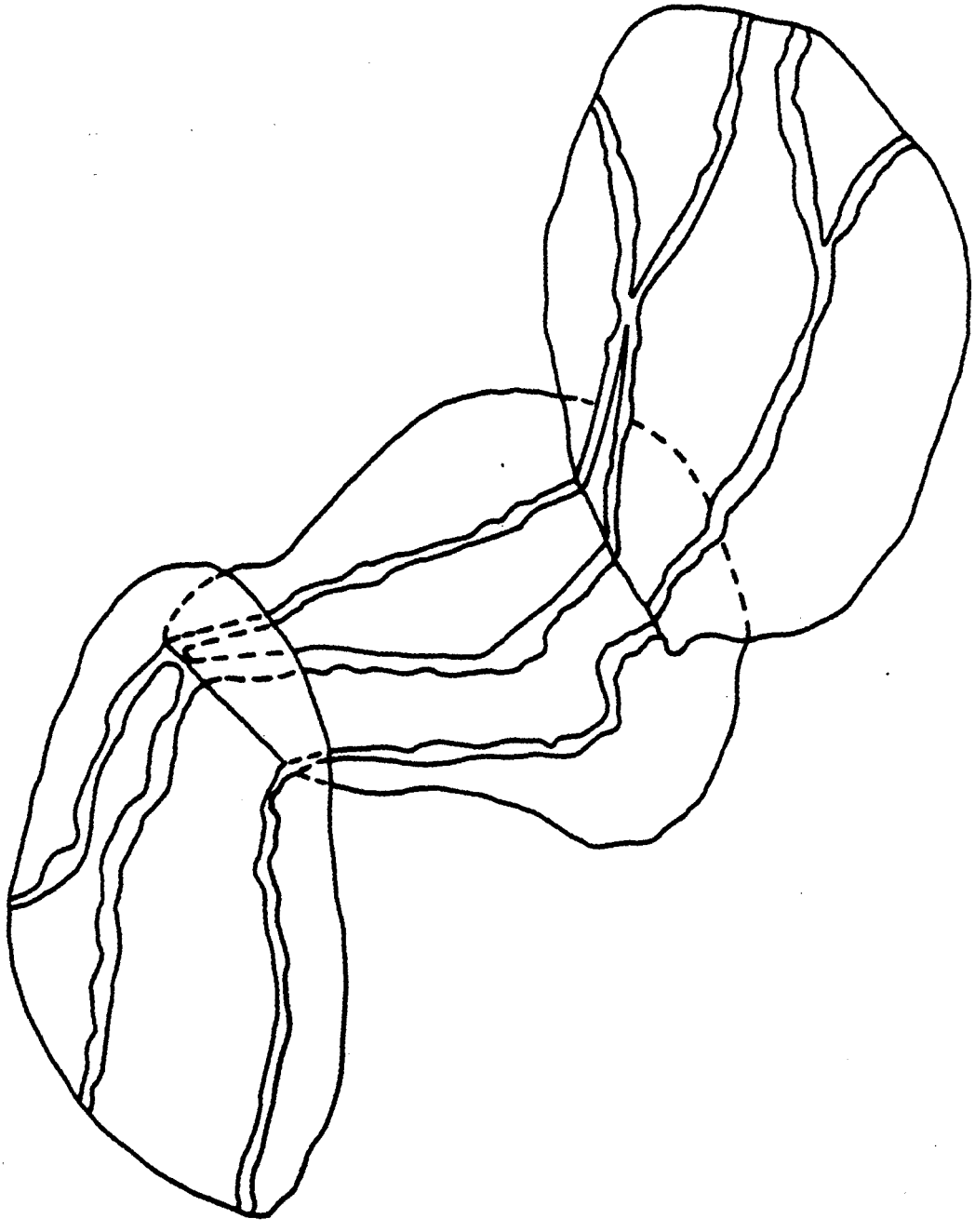

XBL 863-10711

Figure 2.

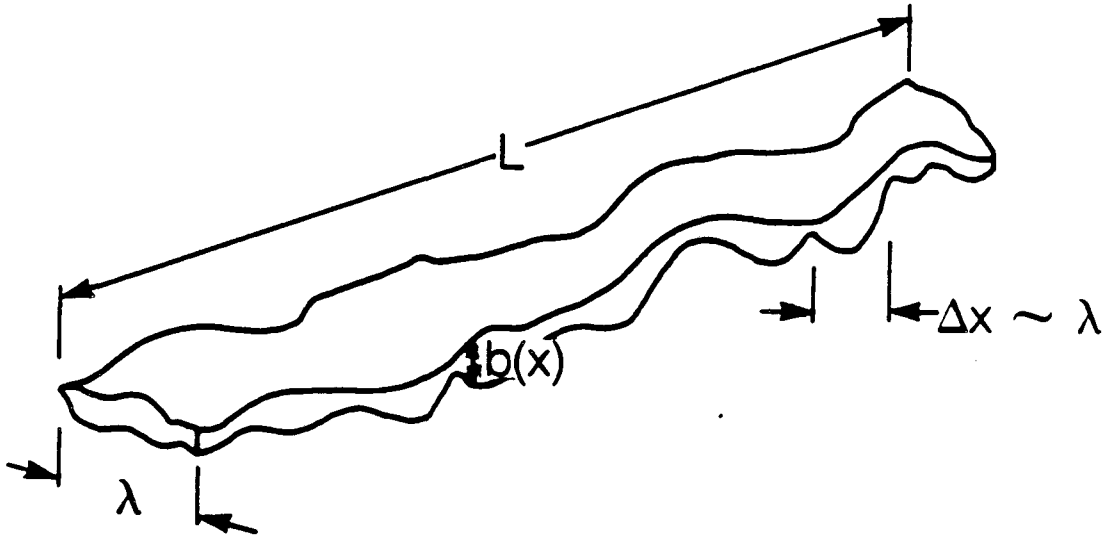

XBL 863-10710

Figure 3.

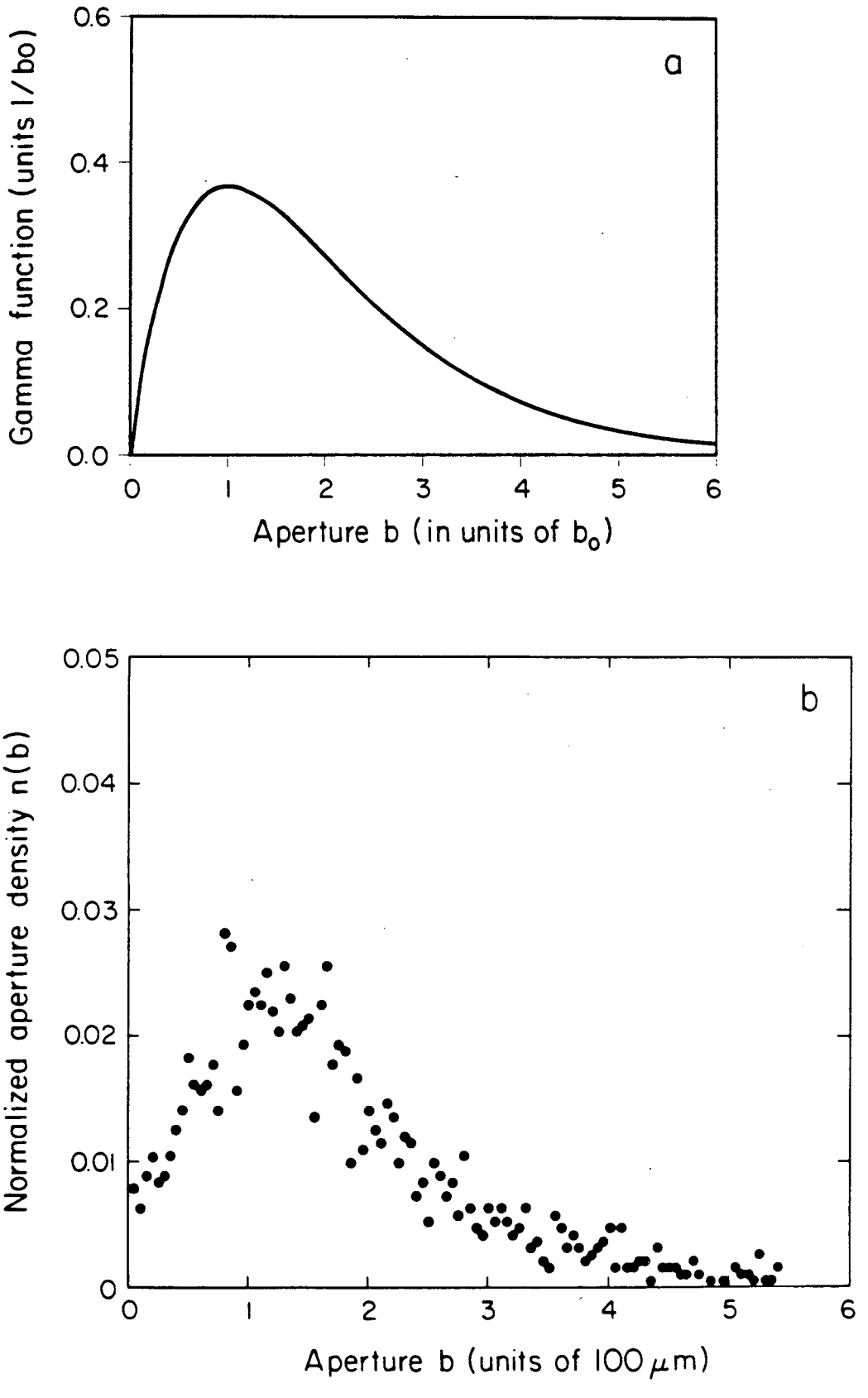

Figure 4.

XBL 841-9556

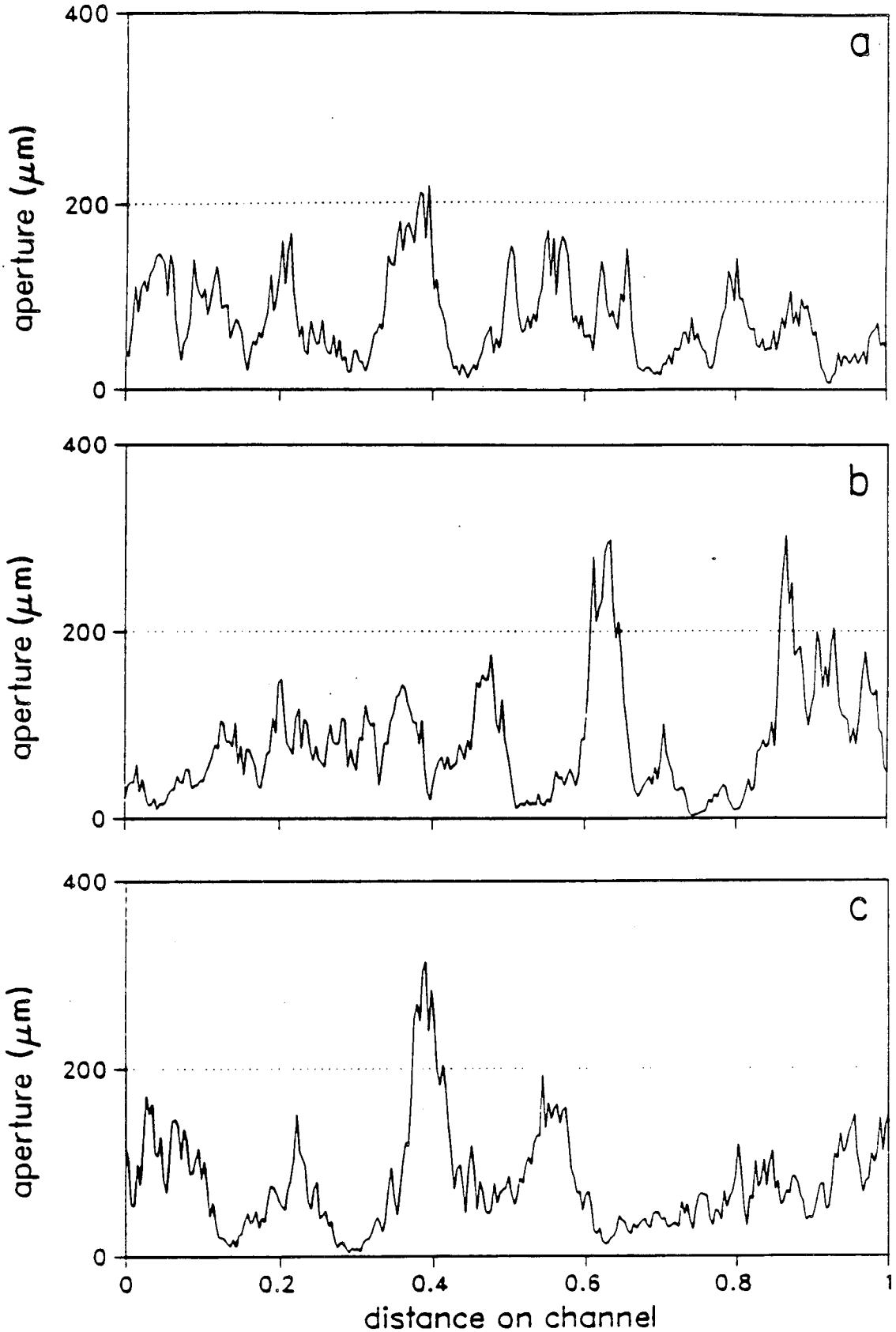
correlation 0.15
400
200
0
aperture (μm)
a
b
c
0
0.2
0.4
0.6
0.8
1
distance on channel
XBL 863-10720

Figure 5.

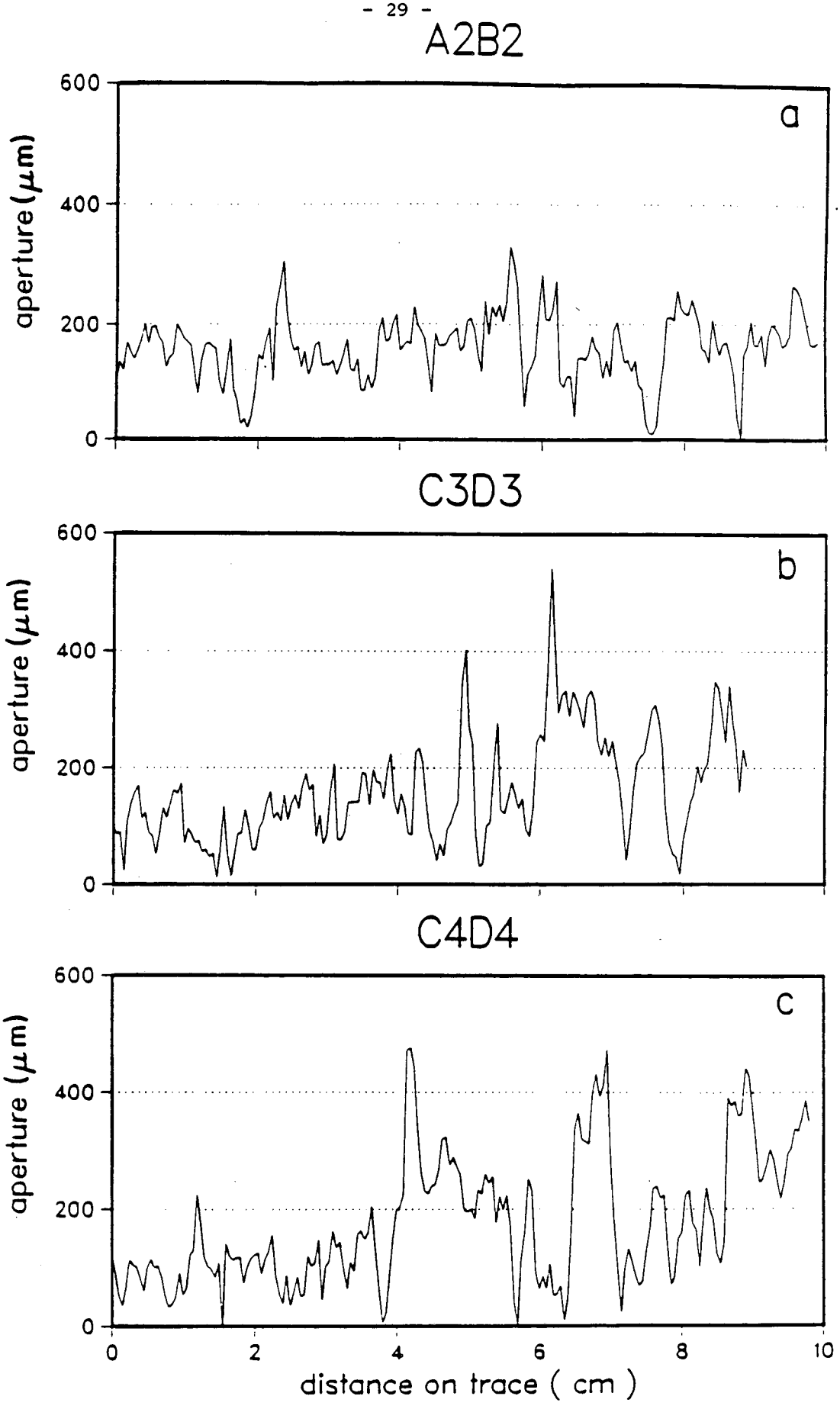

Figure 6.

XBL 863-10730

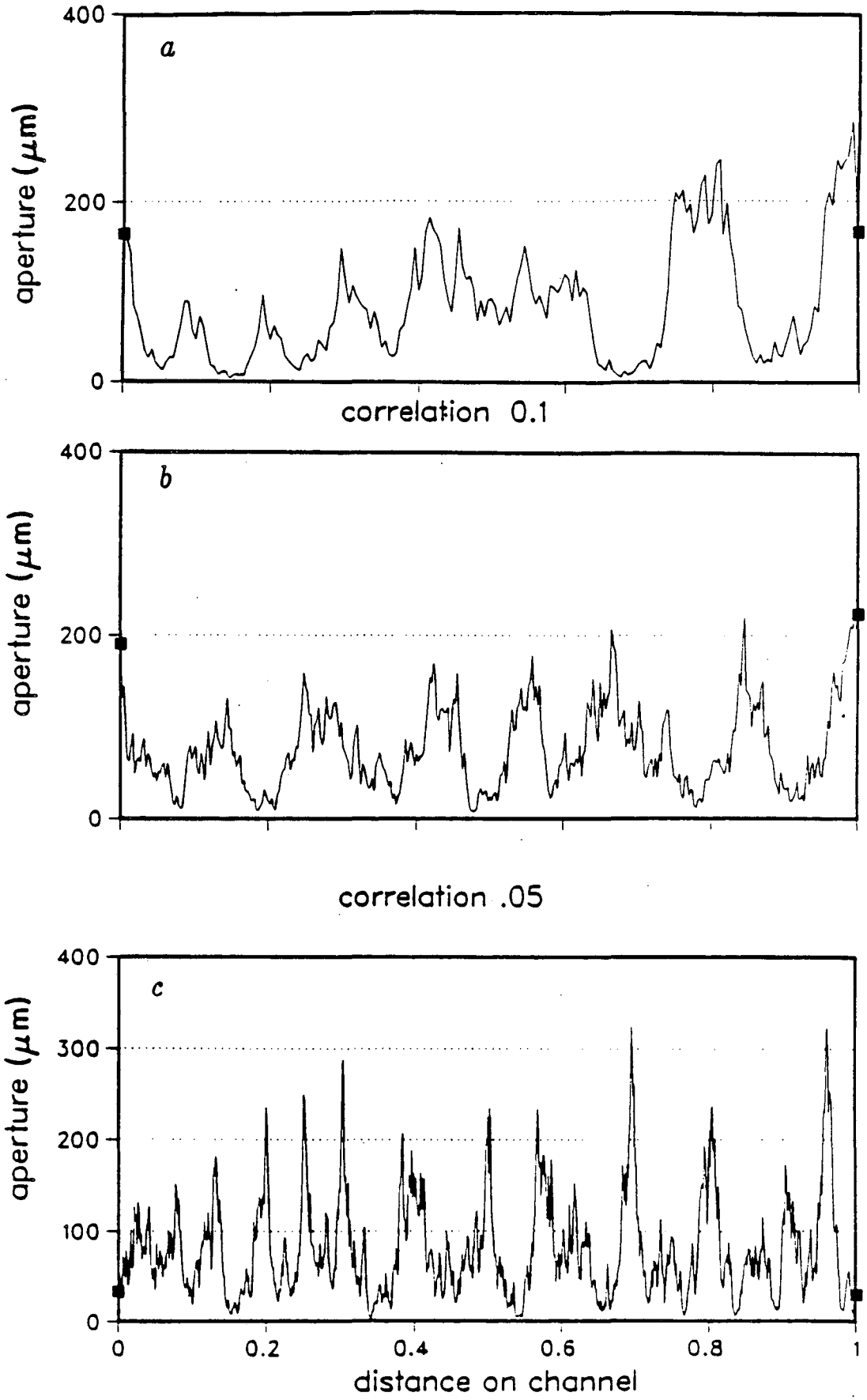

Figure 7.

XBL 863-10731

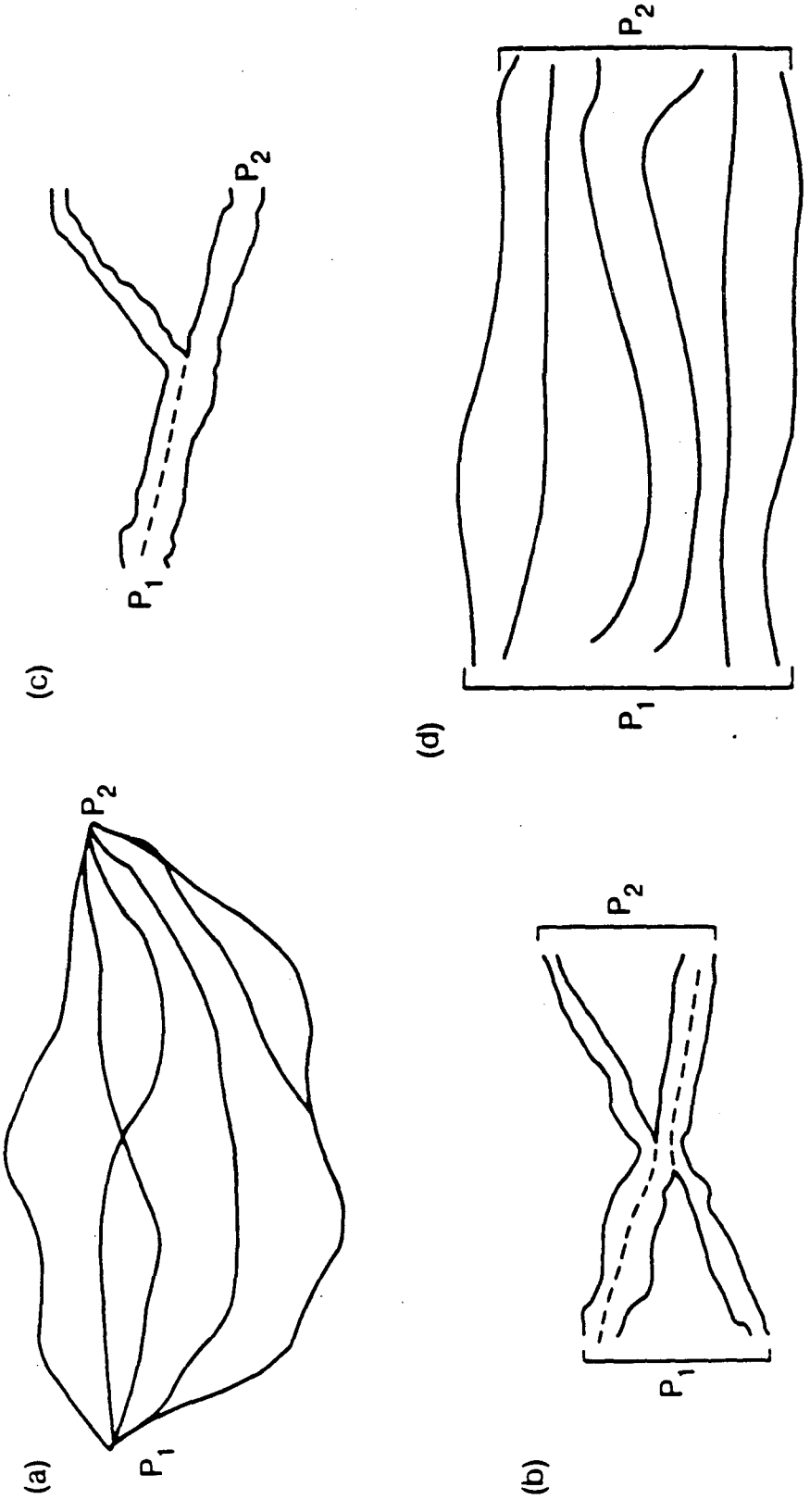

XBL 863-10712

Figure 8.

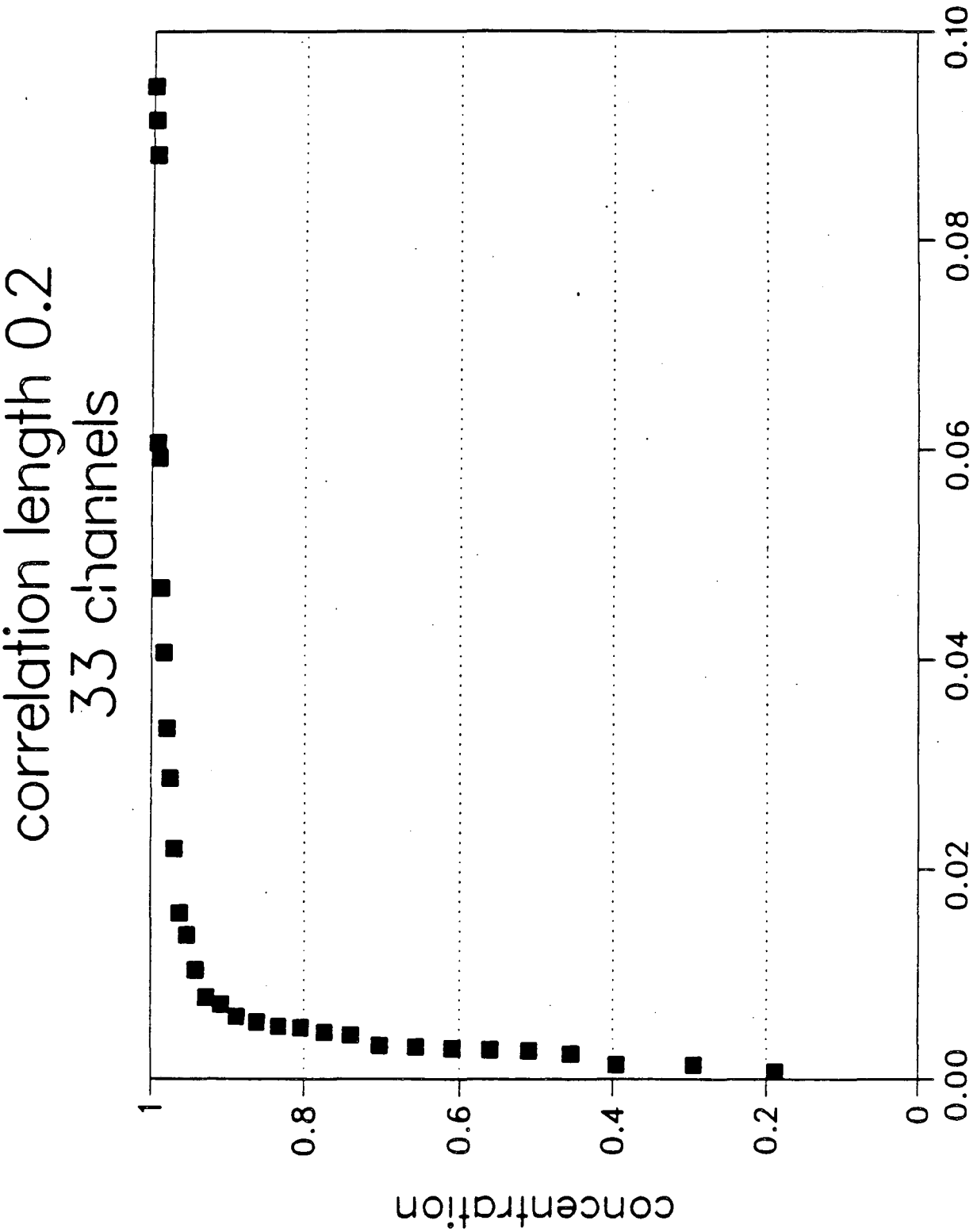
correlation length 0.2
33 channels
concentration
1
0.8
0.6
0.4
0.2
0
0.00
0.02
0.04
0.06
0.08
0.10
time

Figure 9a.

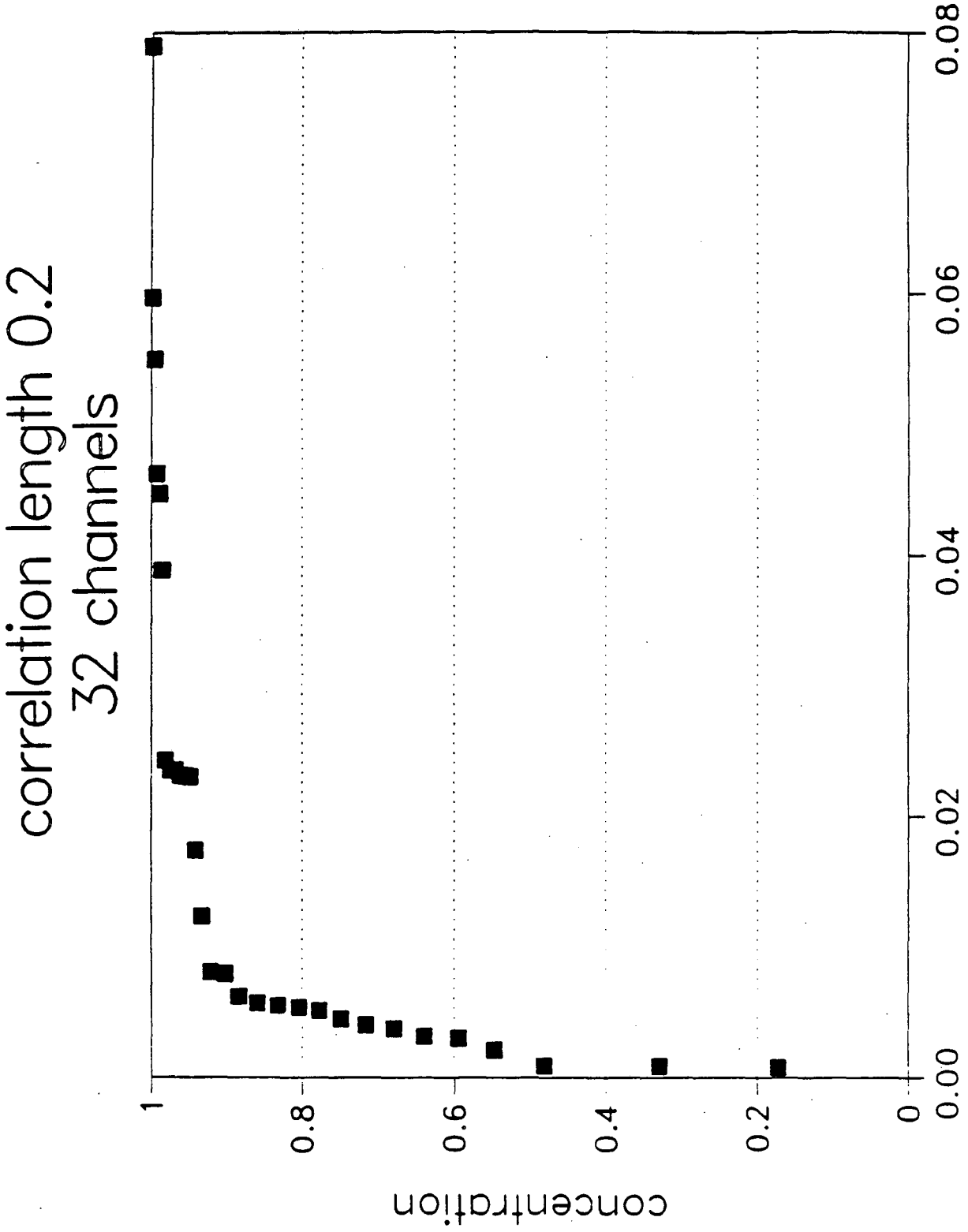
correlation length 0.2
32 channels
concentration
1
0.8
0.6
0.4
0.2
0
0.00
0.02
0.04
0.06
0.08
time

Figure 9b.

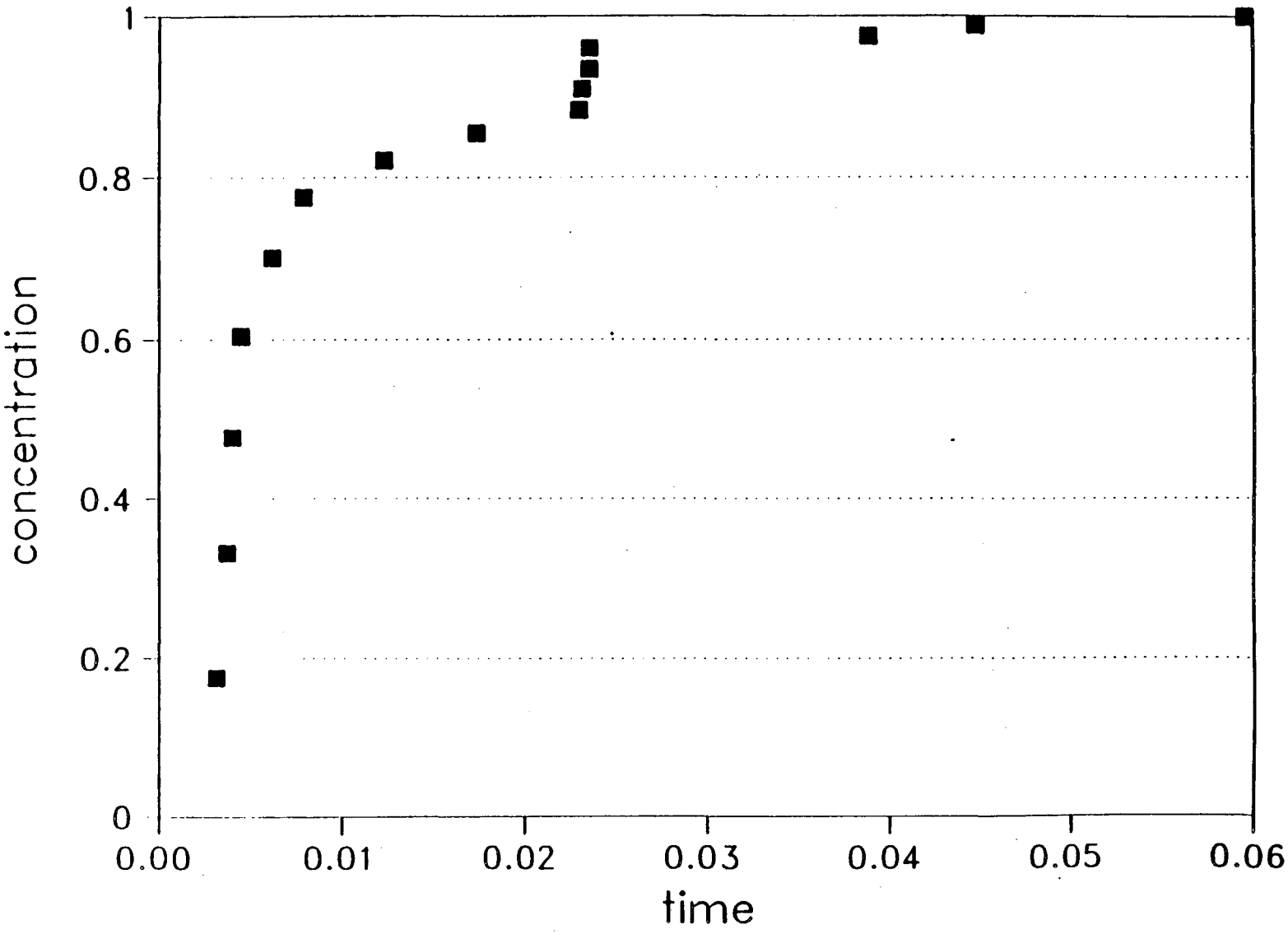
correlation length 0.2
16 channels
concentration
1
0.8
0.6
0.4
0.2
0
0.00
0.01
0.02
0.03
0.04
0.05
0.06
time

Figure 9c

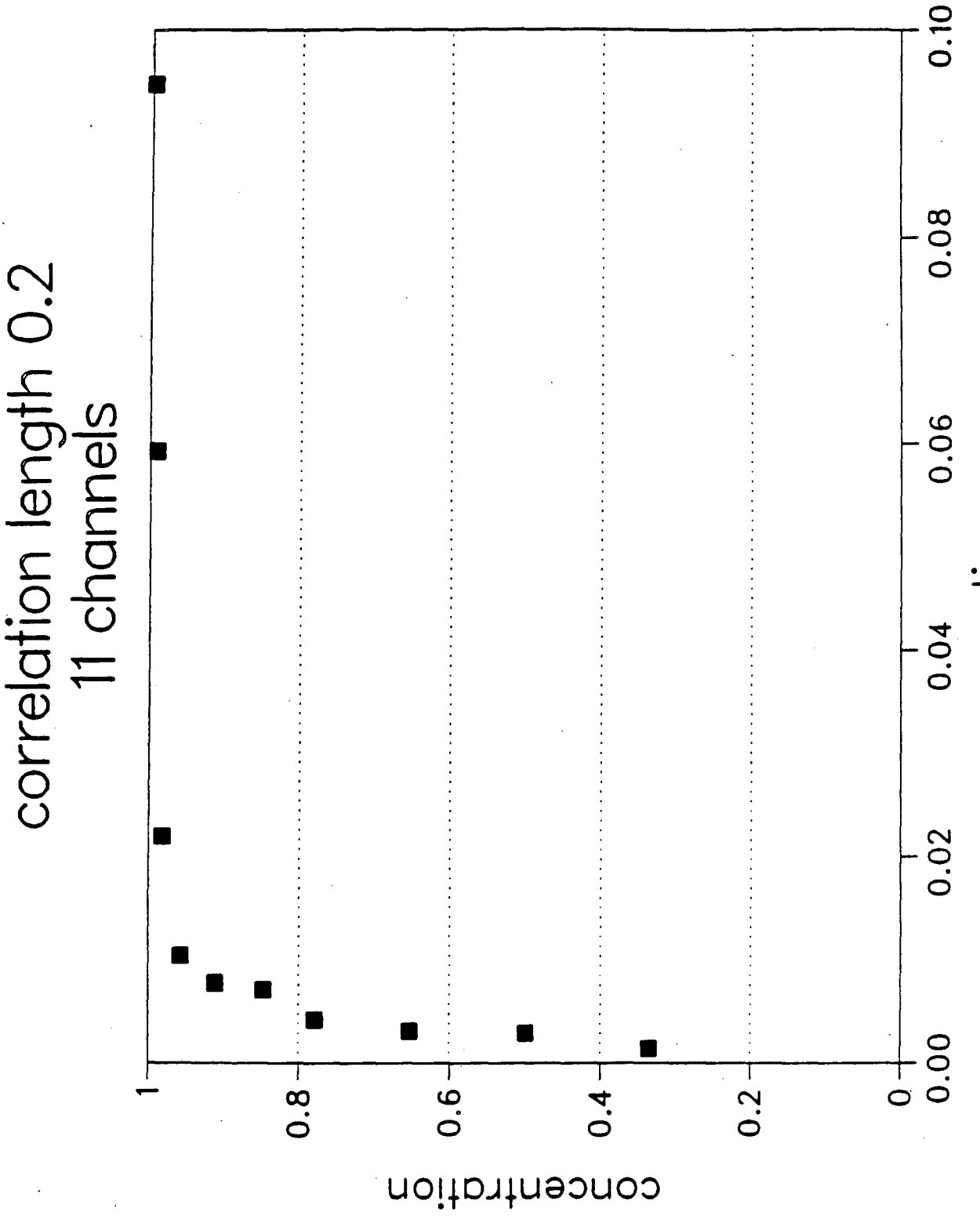
correlation length 0.2
11 channels
concentration
1
0.8
0.6
0.4
0.2
0
0.00
0.02
0.04
0.06
0.08
0.10
time

Figure 9d

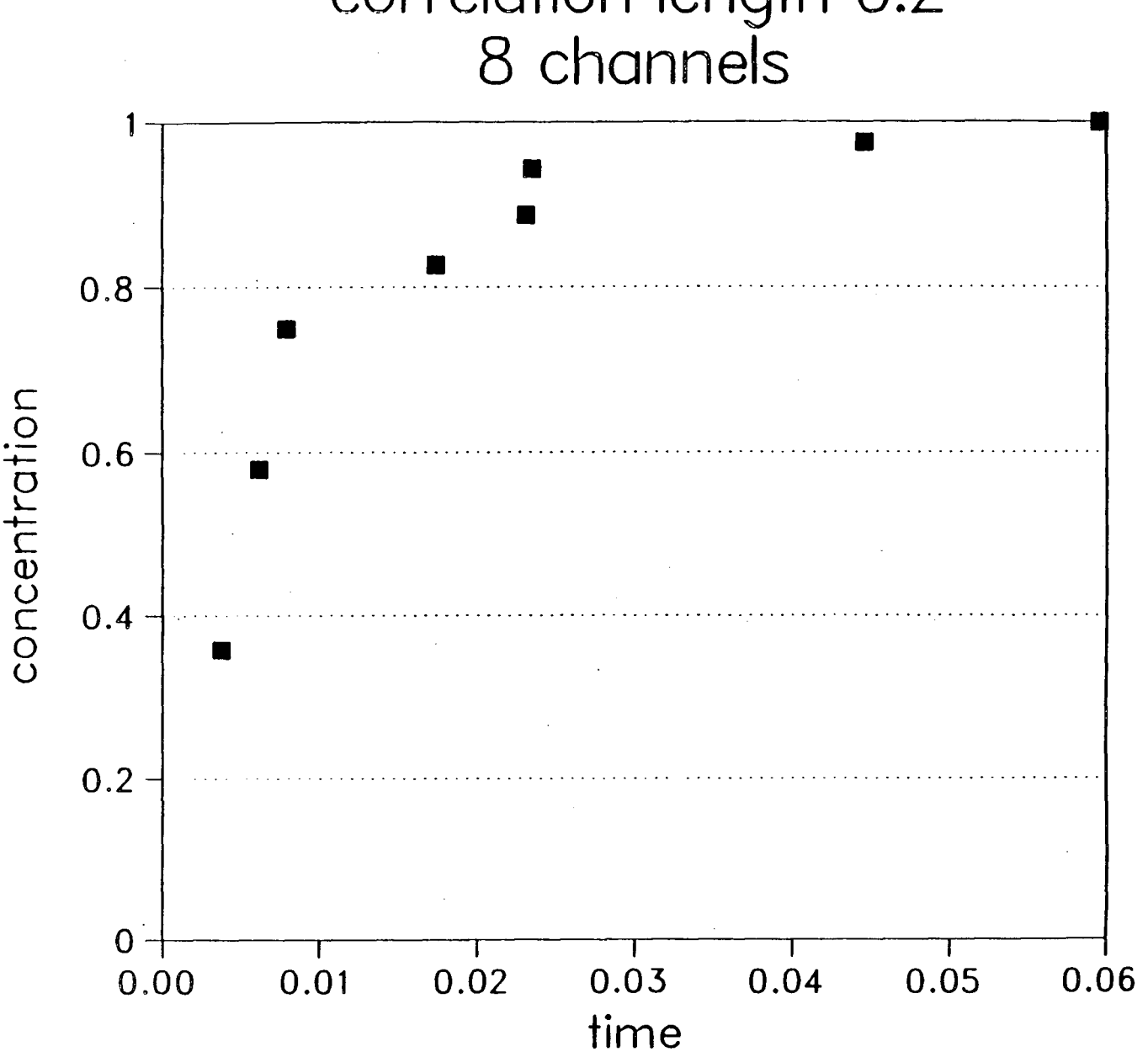
correlation length 0.2
8 channels
concentration
1
0.8
0.6
0.4
0.2
0
0.00
0.01
0.02
0.03
0.04
0.05
0.06
time

Figure 9e

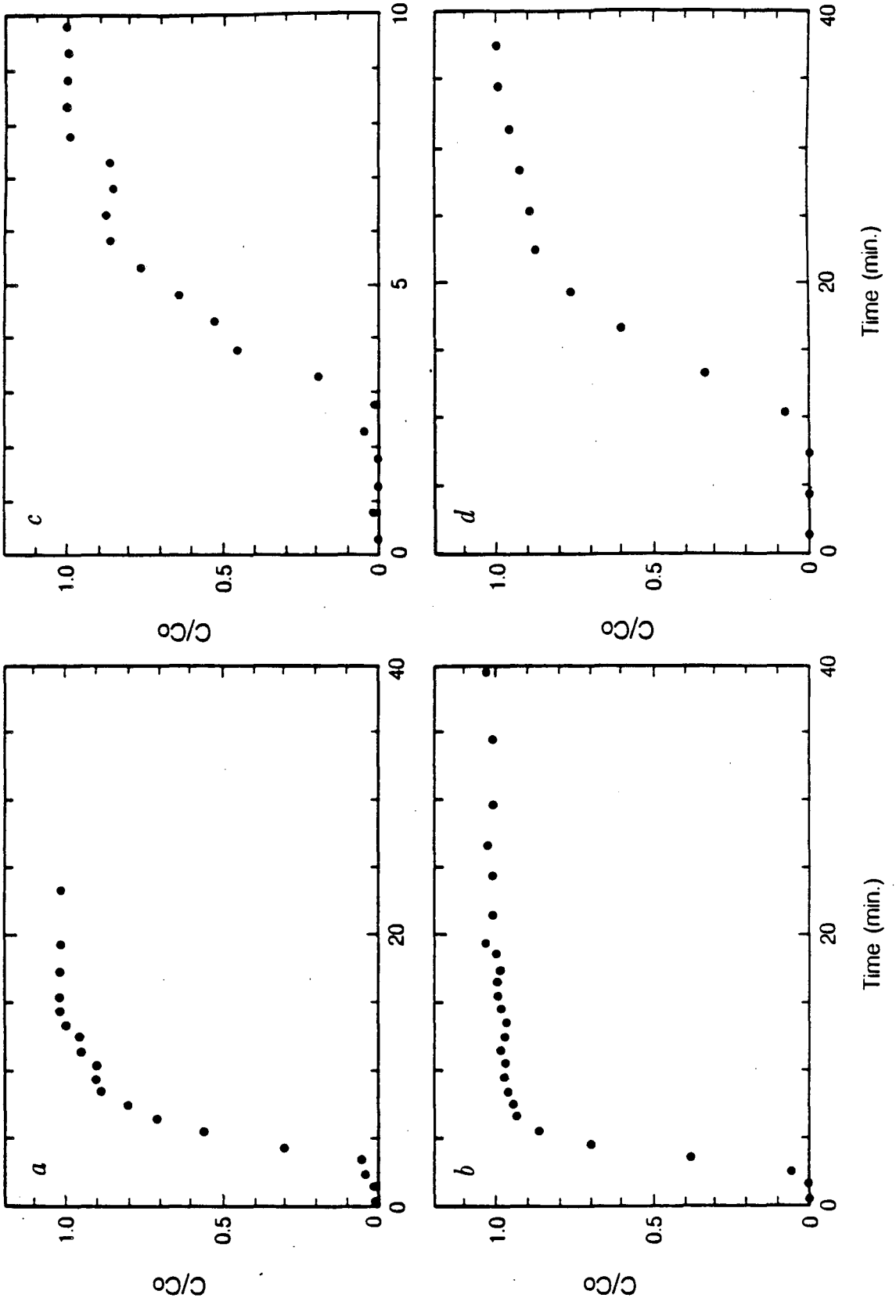

Figure 10.

XBL 863-10713

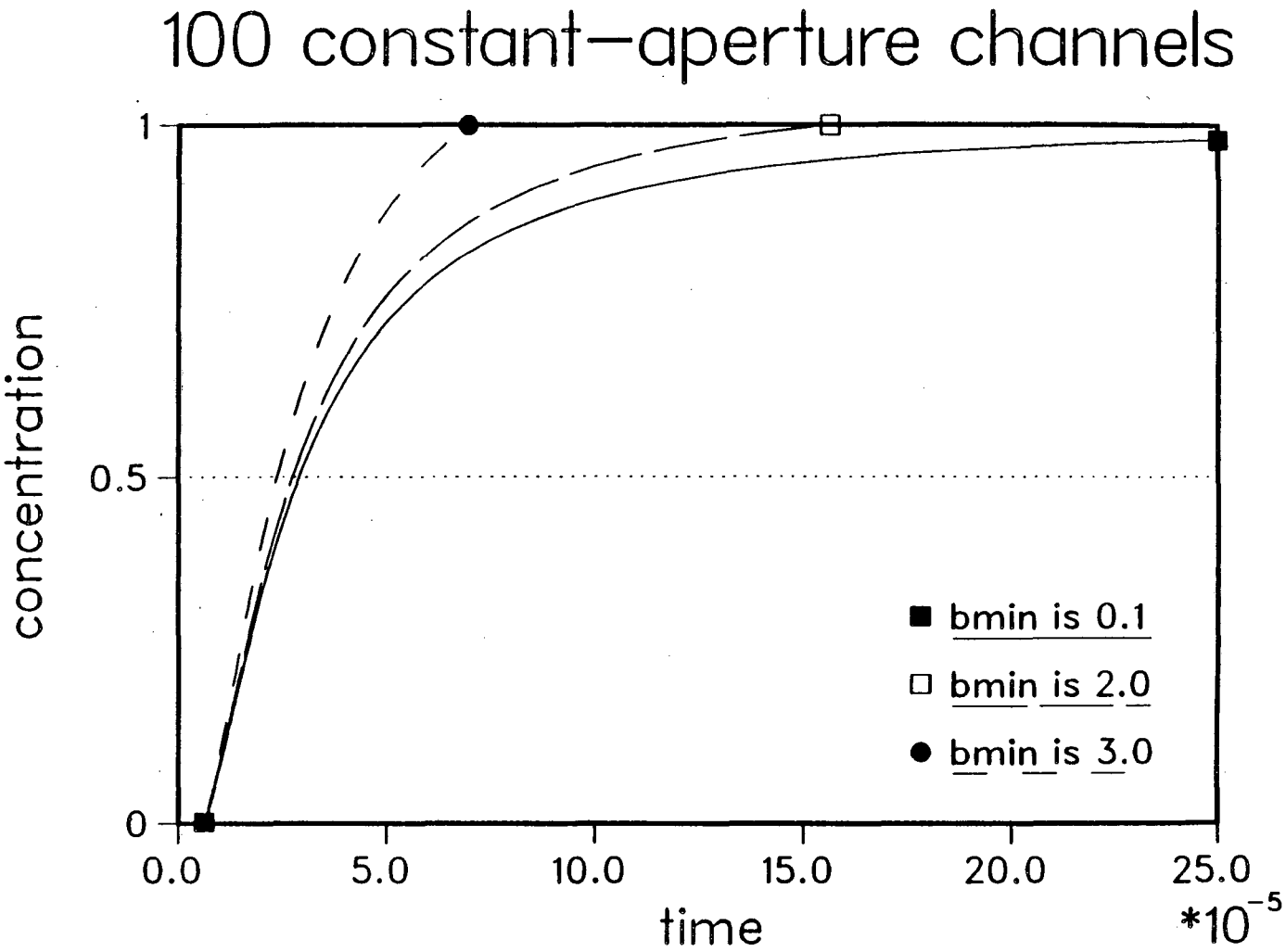

XBL 863-10719

Figure 11.

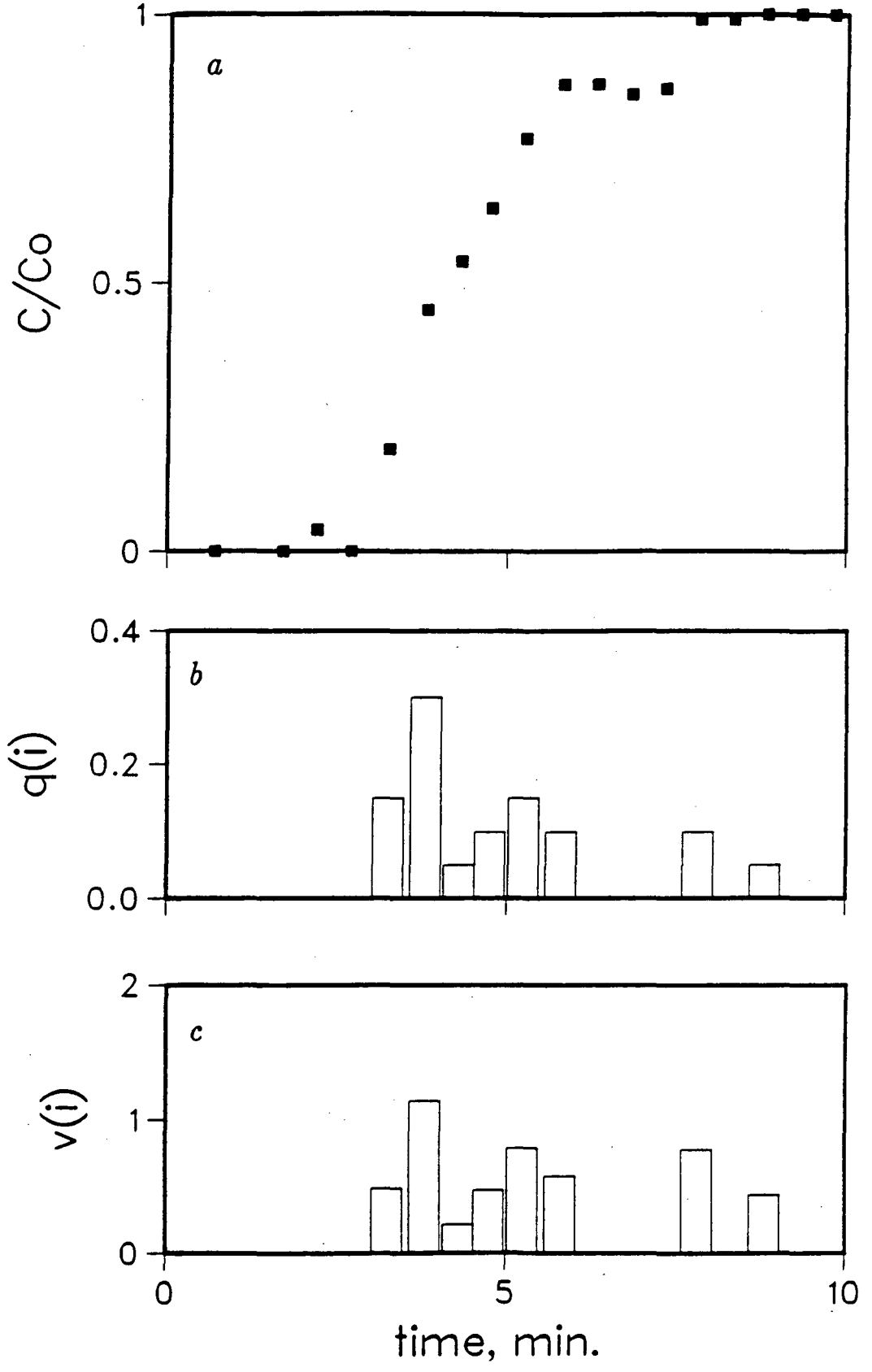

Figure 12

XBL 863-10728

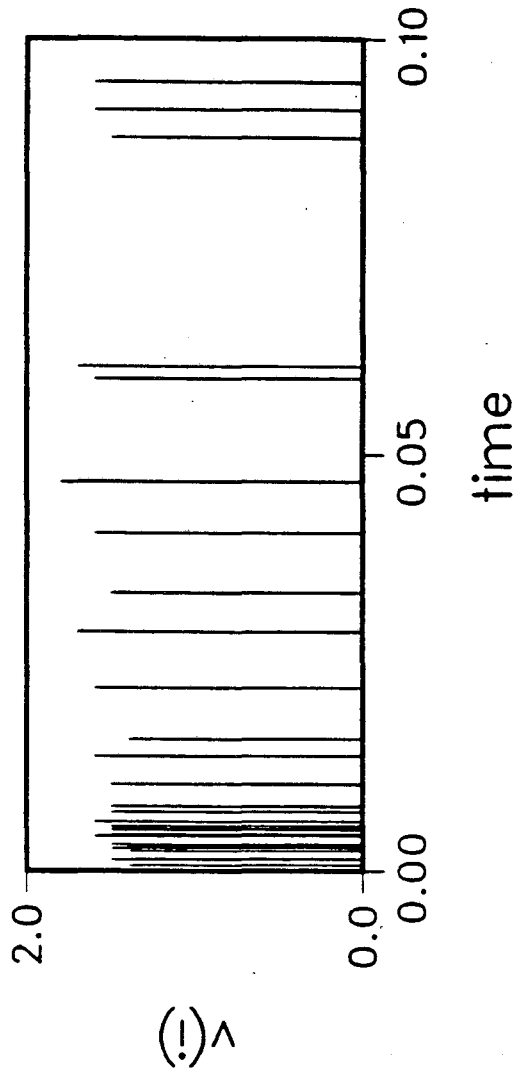

XBL 863-10718

Figure 13

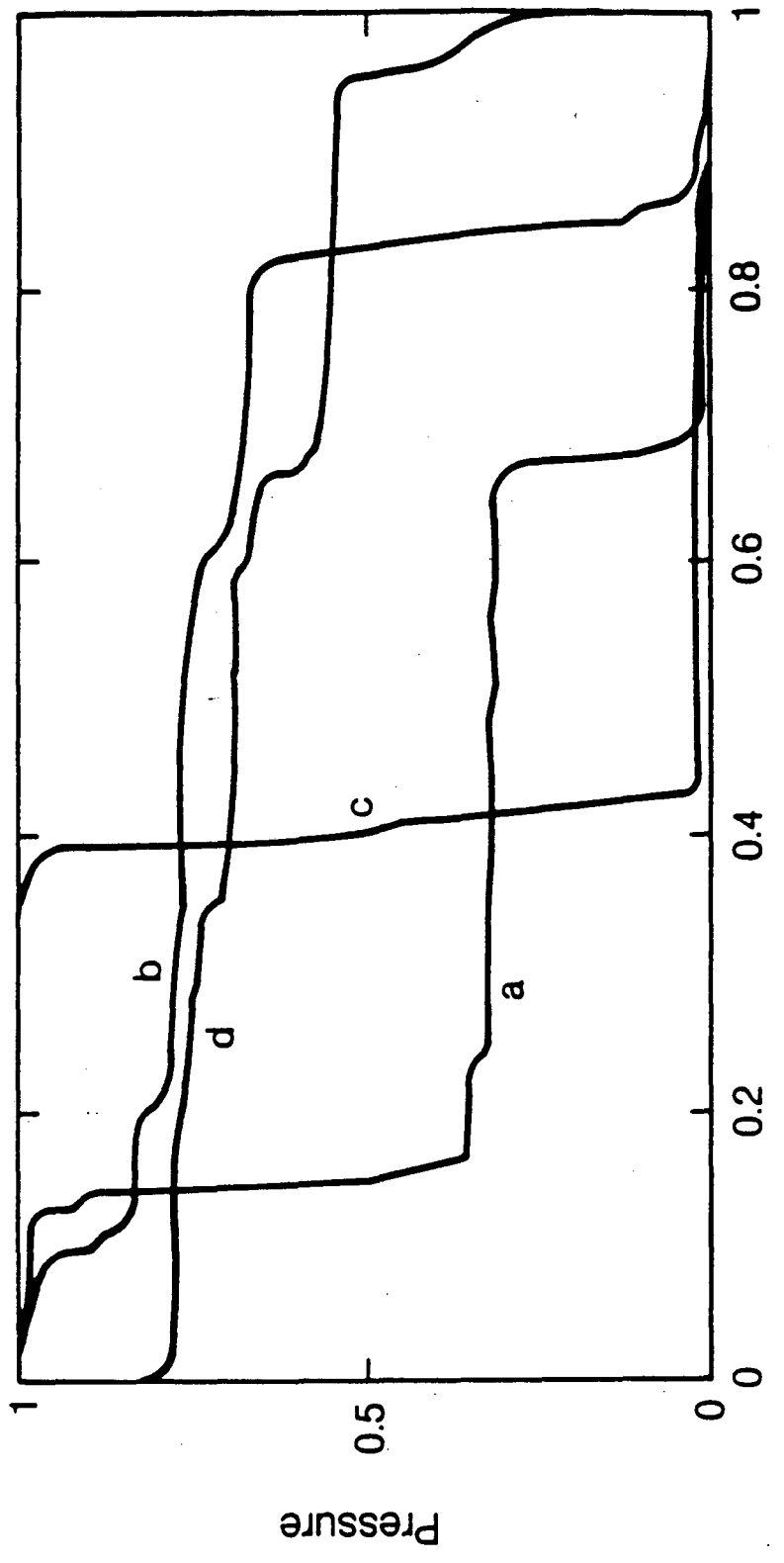

XBL 863-10716

Figure 14

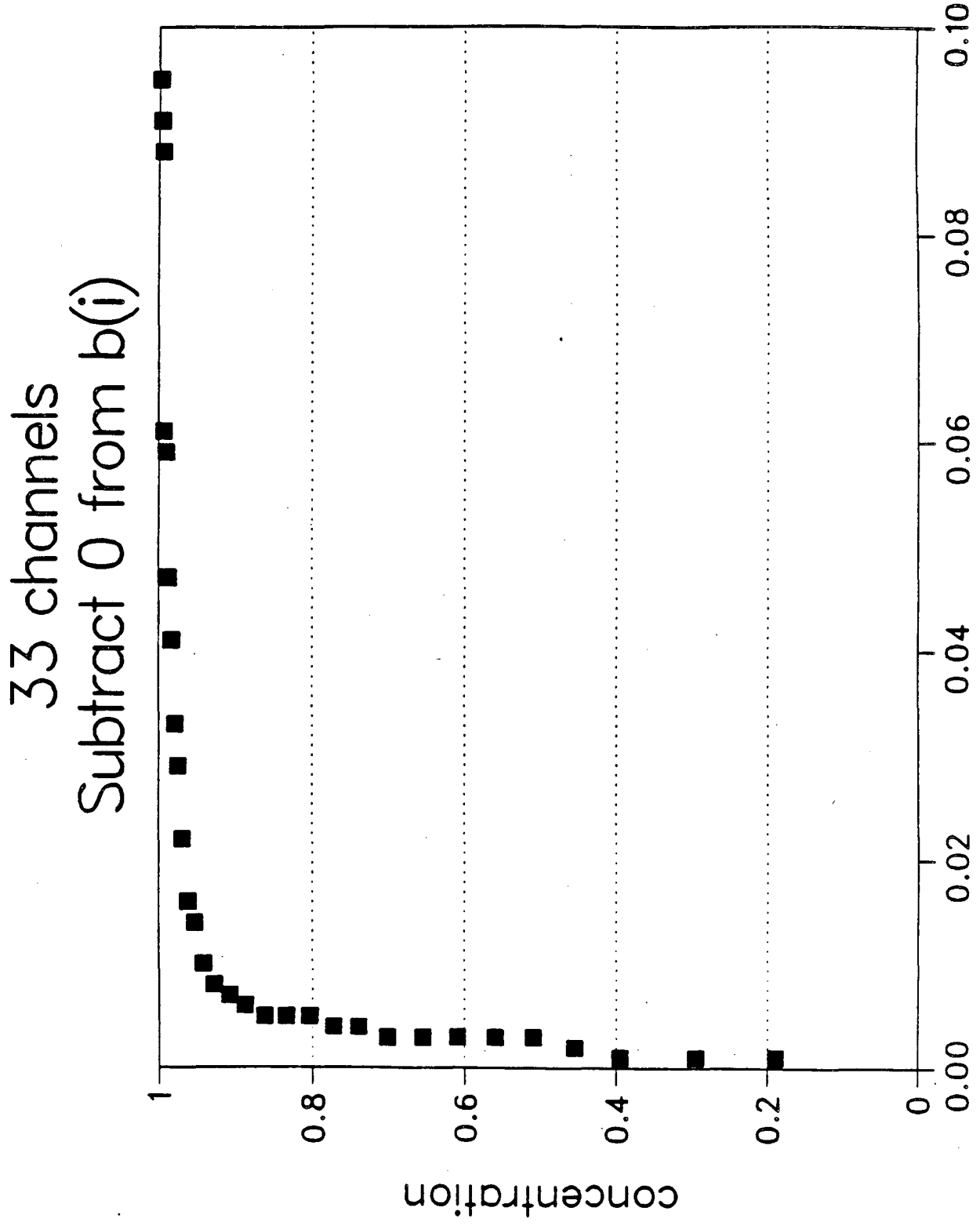
33 channels
Subtract 0 from b(i)
concentration
1
0.8
0.6
0.4
0.2
0
0.00
0.02
0.04
0.06
0.08
0.10
time

Figure 15a

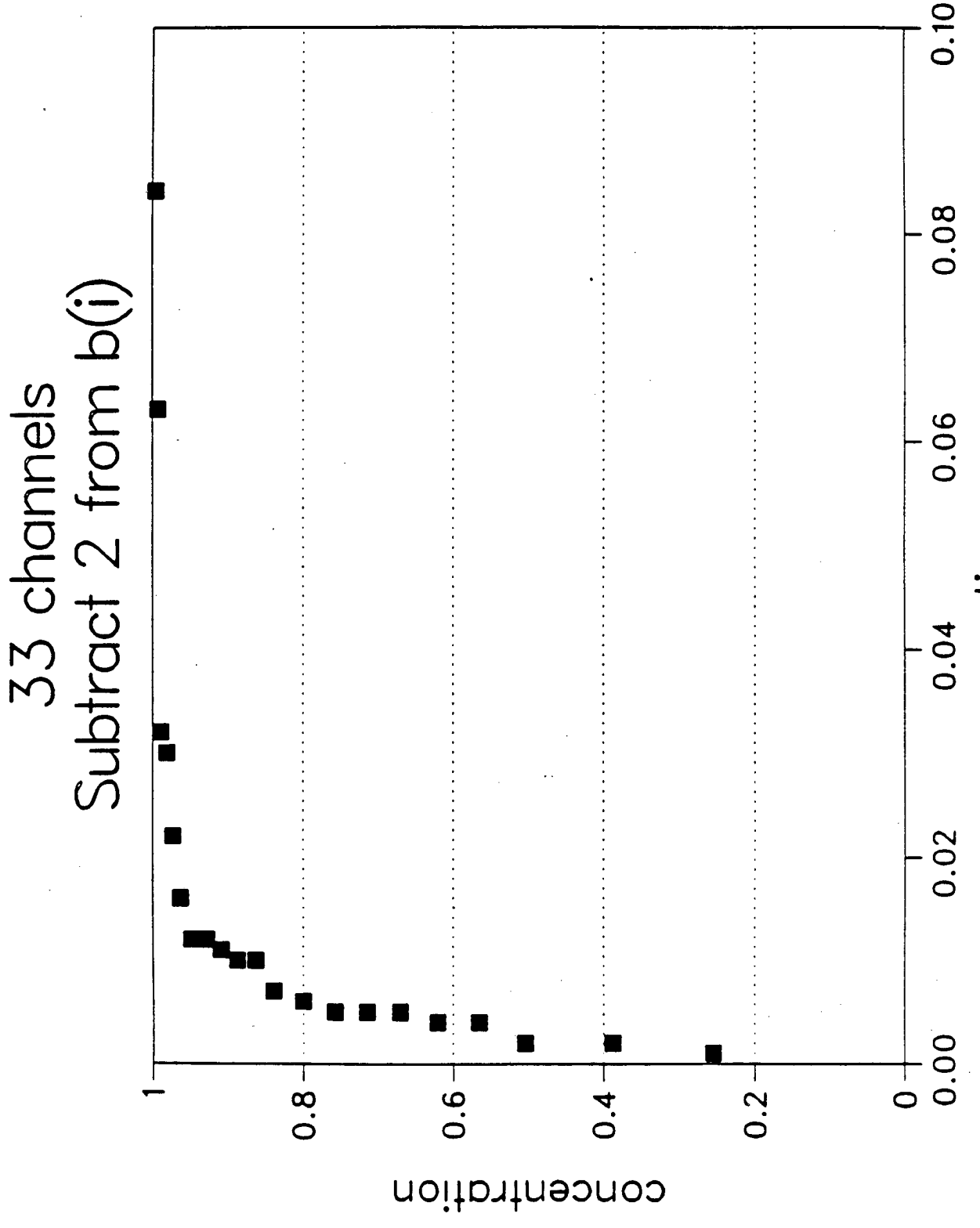
33 channels
Subtract 2 from b(i)
concentration
1
0.8
0.6
0.4
0.2
0
0.00
0.02
0.04
0.06
0.08
0.10
time

Figure 15b

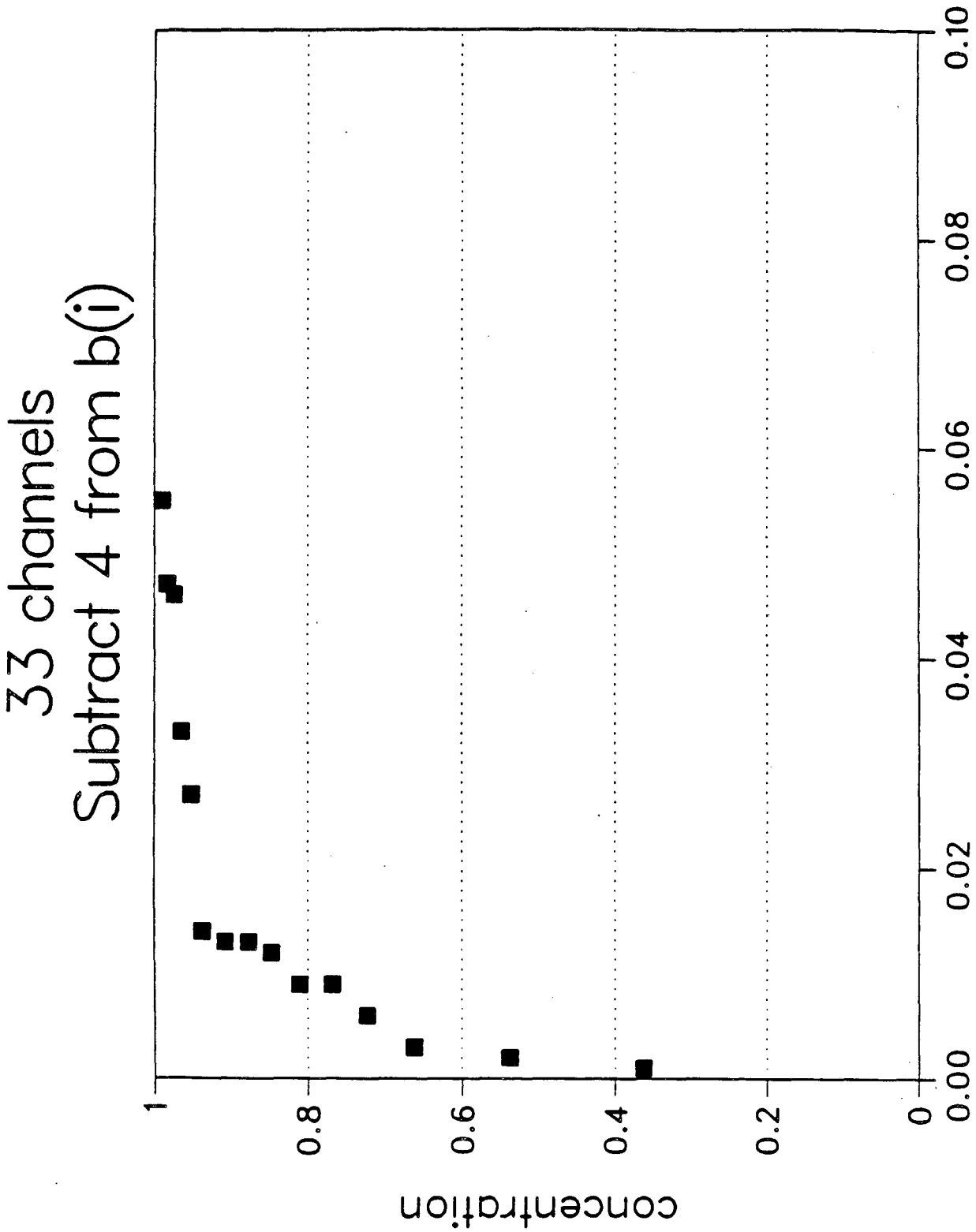
33 channels
Subtract 4 from b(i)
concentration
time
0
0.2
0.4
0.6
0.8
1
0.00
0.02
0.04
0.06
0.08
0.10

Figure 15c

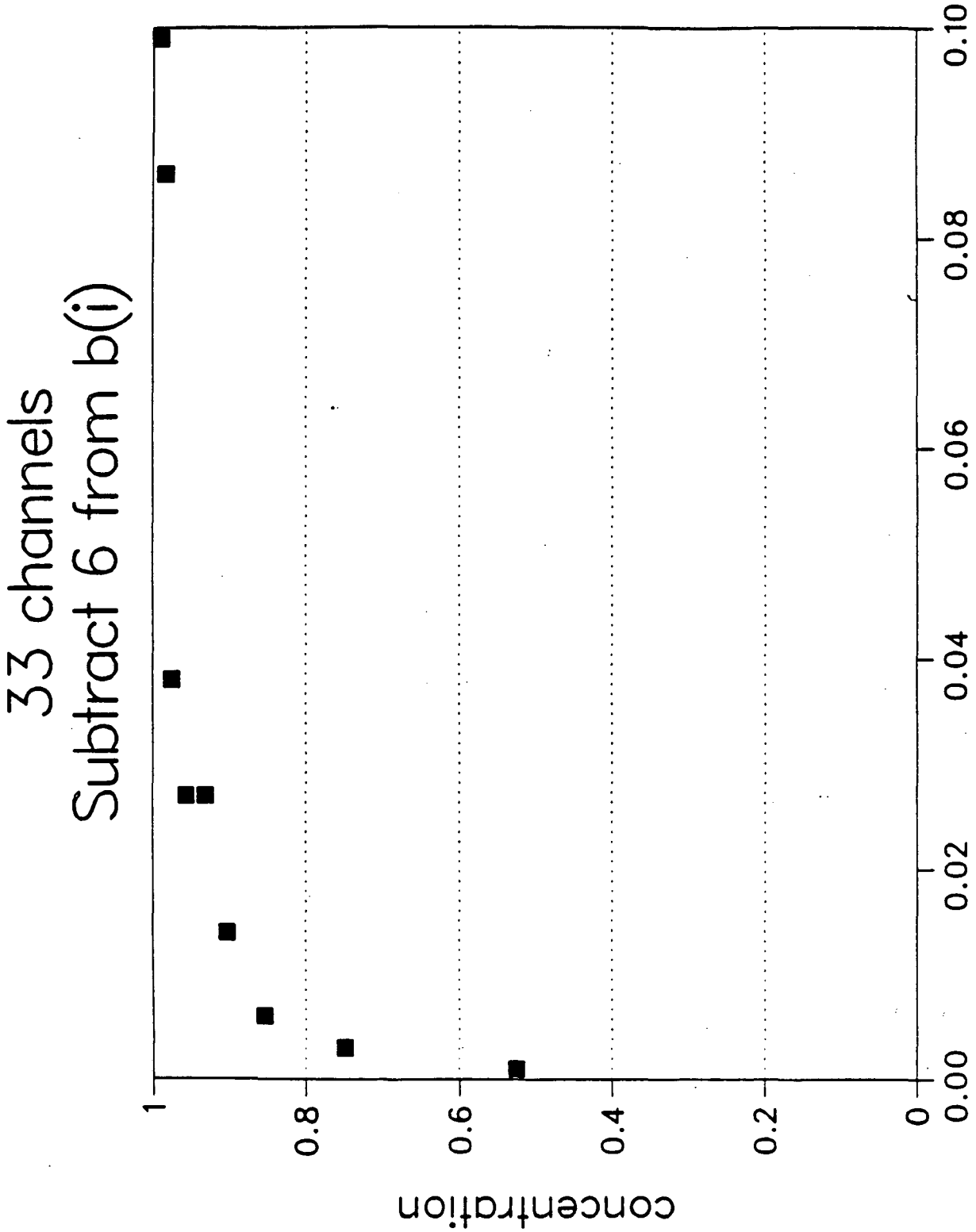
33 channels
Subtract 6 from b(i)
concentration
time
0
0.2
0.4
0.6
0.8
1
0.00
0.02
0.04
0.06
0.08
0.10

Figure 15d

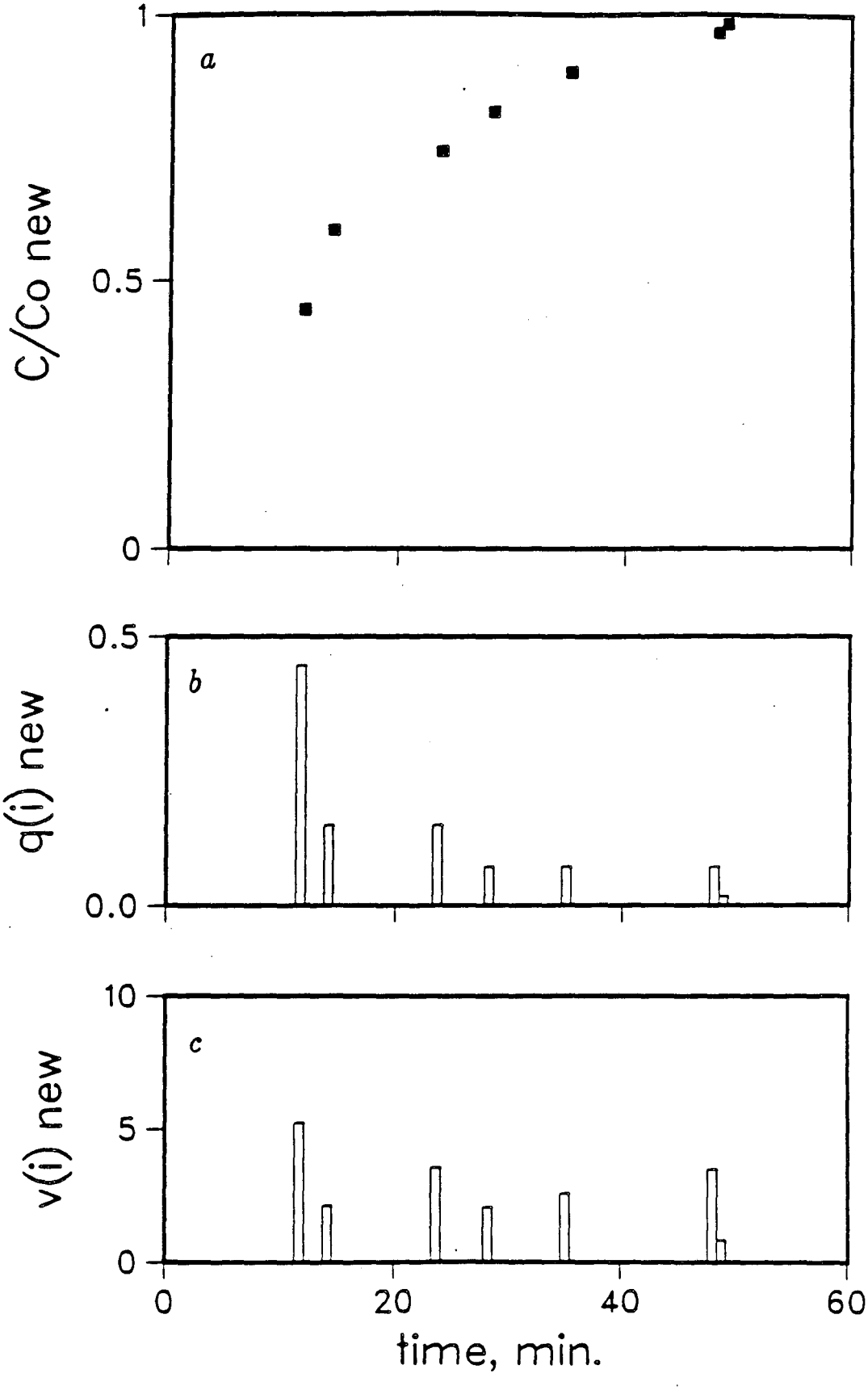

XBL 863-10729

Figure 16

LAWRENCE BERKELEY LABORATORY
TECHNICAL INFORMATION DEPARTMENT
UNIVERSITY OF CALIFORNIA
BERKELEY, CALIFORNIA 94720